MASTER'S THESIS

Design and Implementation of a Fuzzy Adaptive Sliding-Mode Voltage Control System for Three-Phase UPS Inverter

by

Khawar Naheem

Advisor: Professor Jin-Woo Jung

Division of Electronics and Electrical Engineering

Graduate School

Dongguk University-Seoul

2014

Design and Implementation of a Fuzzy Adaptive Sliding-Mode Voltage Control System for Three-Phase UPS Inverter

by

Khawar Naheem

Advisor: Professor Jin-Woo Jung

2014

A Thesis Submitted in Partial Fulfillment of the Requirements for the Degree of Master of Engineering

Approved by:

Professor Han Ho Choi (인)

Professor Keum Cheol Hwang (인)

Professor Jin-Woo Jung (인)

Division of Electronics and Electrical Engineering

Graduate School

Dongguk University-Seoul

Acknowledgements

I would like to express my deep and sincere gratitude to my Advisor Prof. Jin-Woo Jung for the continuous support of my master's study and research, for his patience, motivation, enthusiasm, and immense knowledge. His guidance, constructive comments and suggestions helped me in all the time of research and writing of this thesis.

I appreciate the kindness and moral support of all my laboratory mates: Dr. Nga Thi-Thuy Vu, Dr. Viet Quoc Leu, Dr. Ton Duc Do, Mr. Dong-Young Yu, Mr. Young-Sik Choi, Mr. Jackson John Justo, Mr. Dong Quang Dang, Mr. Francis Mwasilu, Ms. Eun-Kyung Kim, Mr. Saad Rafaq, and Mr. Hyuk Choi. We worked as a team by helping each other and enjoying every moment together.

I owe sincere and earnest thankfulness to the Dongguk University and its staff for the academic, technical, and financial support, particularly in the award of a "Study and Research at Dongguk University (SRD) Scholarship" that provided the necessary financial support for this research. Also, the facilities of "Distributed Generation Systems and Power Conversion Applications (DGS & PCA) Laboratory" have been indispensable.

Last but not least, I would like to take this opportunity to express my thanks to my family members, especially my parents, for their prayers, encouragement, endless love, and supporting me spiritually throughout my life.

Abstract

Design and Implementation of a Fuzzy Adaptive Sliding-Mode Voltage Control System for Three-Phase UPS Inverter

---

Name: Khawar Naheem

Advisor: Prof. Jin-Woo Jung

Division of Electronics and Electrical Engineering

Dongguk University

Nowadays, the nonlinear nature of electric loads leads to a strong demand of a high-quality and reliable power source both by the customers and utilities. To address this issue, the uninterruptible power supplies (UPSs) are extensively employed for the critical loads such as communication systems (i.e., data centers), medical support systems, semiconductor manufacturing systems, etc. For improving the power quality using UPS system, it is important to achieve the sinusoidal output voltage waveform with very low total harmonic distortion (THD) regardless of the load types. Typically, the inverter with *LC* output filter in the UPS system is a suitable solution to fulfill this requirement. The main criteria to evaluate the regulation performance of the UPS inverter output voltage are fast dynamic response, small steady-state error, and low THD. Furthermore, the various

load conditions (abrupt load changes, unbalanced load, and nonlinear load) including parameters uncertainties extremely degrade the performance of the UPS inverter. Thus, an appropriate control strategy is desired to sufficiently meet the performance criteria of the UPS systems under any type of electrical loads and uncertainties.

This thesis proposes an advanced control approach named as fuzzy adaptive sliding-mode voltage controller (FASVC) for a three-phase UPS inverter. The proposed FASVC is a combination of two artificial intelligent control laws: 1) Fuzzy adaptive control law; 2) Sliding-mode control law. The former one is adopted as the compensation control term, and its duty is to solve the problems of the parameters uncertainties. Whereas the latter one is employed as the feedback control term, and its responsibility is to stabilize the error dynamics of the system. For enhancing the reliability of the whole control system and decreasing the number of current sensors, a conventional load current observer is also utilized. Moreover, the stability of the proposed FASVC is fully guaranteed by using the Lyapunov stability theory.

Finally, the extensive simulation and experimental studies are conducted to validate the excellent performance, such as fast dynamic response, small steady-state error, and low THD, of the proposed FASVC under different case-studies in the existence of the parameters uncertainties. To better judge the superior performance of the proposed control strategy, a conventional sliding-mode control (SMC) method is also implemented under the same conditions. The comparative simulations are carried out by using MATLAB/Simulink software and the comparative experiments are implemented on a prototype 1 kVA three-phase UPS inverter system via TMS320F28335DSP.

Table of Contents

List of Figures

Acronyms

UPS	:	Uninterruptible power supply
FASVC	:	Fuzzy adaptive sliding-mode voltage controller
SMC	:	Sliding-mode control
rms	:	Root mean square
VR	:	Voltage regulation
THD	:	Total harmonic distortion
CF	:	Crest factor
VD	:	Voltage-dip
St	:	Settling time
KCL	:	Kirchoff's current law
KVL	:	Kirchoff's voltage law
SVPWM	:	Space vector pulse width modulation
IGBT	:	Insulated gate bipolar transistor
L_f	:	Filter inductance
C_f	:	Filter capacitance
VSC	:	Variable structure control
RLC	:	Resistance, inductance, and capacitance

Chapter 1: Introduction

This chapter expresses the power quality issues in the modern power system and introduces an uninterruptible power supply (UPS) as a reliable solution to these issues. It elaborates the main types and performance evaluation criteria for the UPS inverter systems. Also, it reviews the existing advanced control techniques already employed for the UPS inverter systems. Finally, it presents the objective and composition of the thesis.

1.1 Power Quality Issues

In recent years, most of the daily-life devices and equipments are totally dependent on the electric power because it increases the productivity, efficiency, and provides a high degree of safety and comfort of life. Both the quality and interruption of the electric power cannot be tolerated in the critical areas such as safety (air traffic control, hospitals, railway systems etc.), security (military installations, police stations etc.), continuous industrial processes (semiconductor wafer processing plant, cement mill, textile machines, etc.), data protection (internet service providers, banks etc.). So, the stakes are very high for the continuous and clean electric power [1]. For the optimum operation of the power system network, it is important for the power distributors to deliver a sinusoidal voltage waveform of a constant magnitude and constant frequency (typically 110 V per-phase rms, 60 Hz). However, meeting these demands is difficult as the contingencies and power quality issues like harmonics, notching, surges, and sags are frequent and well reported [2], [3].

In fact, the power quality issues are becoming significant due to the proliferation of the nonlinear loads such as rectifier equipments, adjustable speed drives, domestic appliances, and arc furnaces. These nonlinear loads draw non-sinusoidal/distorted currents from utility and result a high total harmonic distortion (THD) in the output voltage waveforms. Furthermore, the high THD value causes more catastrophic problems in the power system and consumer products like equipment overheating, capacitor blowing, motor vibration, transformer over-heating-excessive neutral currents, and low power factor. For all of these reasons the high quality and reliable power increasing concerns to both the utilities and their customers [4]-[8]. Therefore, a feasible solution is always required to solve the power quality issues.

1.2 Uninterruptible Power Supply (UPS)

To improve the quality and reliability of the power source, the uninterruptible power supply (UPS) systems are widely employed as a suitable solution. Acting as an interface between the mains and sensitive applications, the UPSs feed the load with continuous and clean electrical power regardless of the status of the mains [9]. The UPS systems not only protect the sensitive loads against power interruption, over-voltage (surge), and under-voltage (sag) conditions, but also suppress the power line transients and harmonic disturbances. Generally, an ideal UPS should provide the following features to the utilities and their customers [10]:

- Regulated sinusoidal output voltage with low Total Harmonic Distortion (THD) independent from the changes in the input voltage or in the load;
- Continuous operation that means zero switching (transitioning) time from normal to back-up mode and vice versa;
- Low Electro-Magnetic Interference (EMI) and acoustic noise;

- Low maintenance cost, and small weight and size.

1.2.1 UPS Types

The UPS can be divided into the following three main types [11]: on-line UPS, off-line UPS, and line-interactive UPS.

1. *On-line UPS*: The block diagram of the on-line UPS is presented in Fig. 1-1. It is the most commonly used UPS system. During the normal mode of operation, the rectifier converts the AC input line voltage to DC voltage and then continuously supplies the DC bus, and charges the backup battery. The inverter is connected in series with the load and continuously supplies energy to it. In case of any failure in the utility, the rectifier stops the operation and the inverter draws back-up power from the battery without any discontinuity in the output power. On the other hand, the by-pass switch is utilized either for maintenance or for enhancing the energy efficiency when there are no critical loads during certain periods of installation. Since the inverter is continuously active therefore this type of the UPS generates a clean, well-regulated, and stable output.

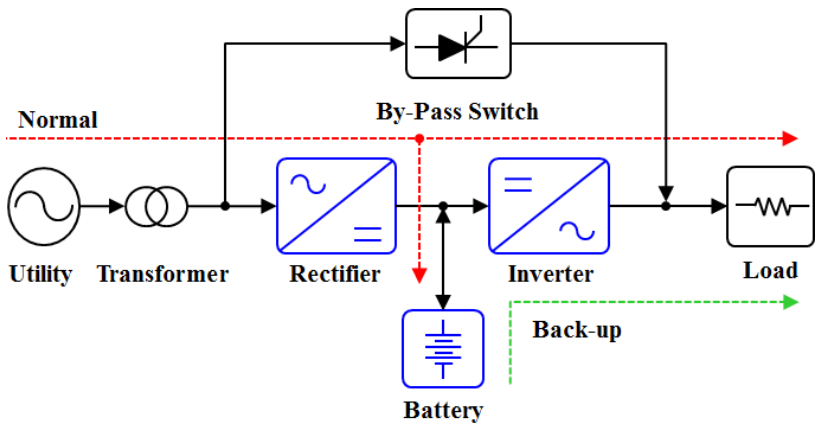

Fig. 1-1 Block diagram of on-line UPS.

2. *Off-line UPS*: This type of UPS is mainly connected in parallel to the load as shown in Fig. 1-2. During normal mode of operation, the by-pass switch is close and provides electric power directly to the load. At the same time, the battery is being charged through the rectifier. However, when any disturbance happens in the power line, the UPS switched in and feed the load through battery back-up. The off-line UPS has advantages of lower cost, smaller size and weight, and higher efficiency; however the slow transition and the low output voltage and frequency regulation are its main disadvantages.

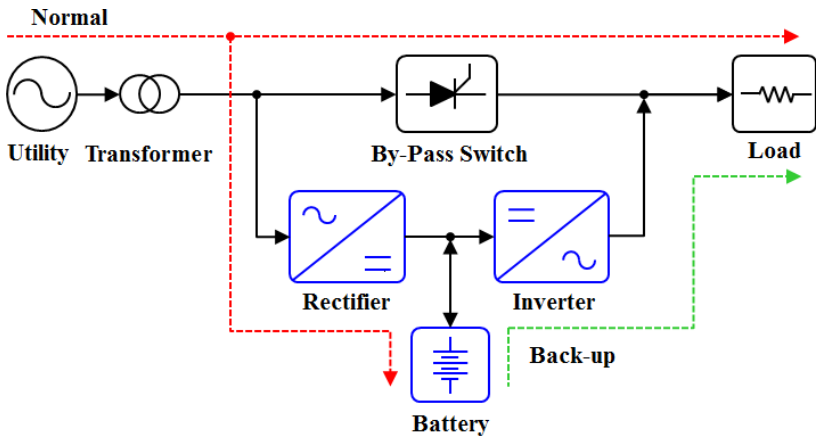

Fig. 1-2 Block diagram of off-line UPS.

3. *Line-interactive UPS*: This configuration of UPS consists of a by-pass switch, a series inductor, a bidirectional converter, and a battery as displayed in Fig. 1-3. In this type, a bi-directional power converter is connected in parallel with the load and operates as a rectifier to charge the battery in the normal-mode. When the AC line fails (like significant voltage sag, interruption etc.), the bi-directional power converter operates as an inverter and supplies the load from the battery. At this moment, the

by-pass switch disconnects the AC line. The line-interactive UPS has better performance than the off-line UPS. One major advantage of the line-interactive UPS systems is their high energy efficiency typically above 95% rated load efficiency. However, the line-interactive UPS does not provide the frequency regulation and the performance totally relies on the energy storage system (battery) during voltage sag conditions.

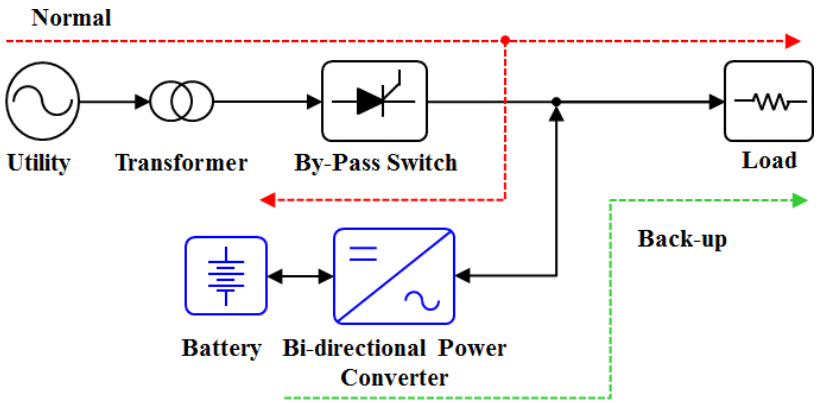

Fig. 1-3 Block diagram of line-interactive UPS.

It is very obvious from the above three UPS types that, at the time of disturbance (i.e., fault, interruption), the UPS system transfer the regulated power to the load through inverter. In many applications, the three-phase inverter is utilized to feed both the single-phase and three-phase loads. Hence, in order to qualify as being regulation performance of the UPS system, the power delivered by its inverter must satisfy the certain requirements/criteria which will be elaborated in the next section.

1.2.2 Performance Evaluation Criteria

The UPS performance can be evaluated through its steady-state and transient-state output voltage characteristics under different load conditions [12].

At steady-state, the nonlinear and unbalanced loads are the most challenging operating conditions. In this regard, the three criterions are: voltage regulation (VR), total harmonic distortion (THD), and crest factor (CF).

1. *Voltage regulation (VR):* It is the percentage deviation of the output voltage from no-load to full-load and is given in (1.1) below, where V_{rrms} is the no-load or reference rms output voltage value and V_{frms} is the full-load or instantaneous rms output voltage value. At steady-state, the output voltage of a UPS inverter should be maintained at V_{rrms} regardless of the operating condition. So, an ideal UPS has zero VR and in a practical UPS a small VR is required. According to the standard IEC 62040-3, the VR for unbalanced load is constrained to 5% (since an unbalanced load poses significant deviations in the output voltage fundamental component). Also, the acceptable VR for balanced linear load is 3% [13]. Typically, the VR of 1% or less is recognized as a high quality UPS. The VR can also be regarded as the steady-state error.

$$VR\% = \frac{V_{frms-}V_{rrms}}{V_{rrms}} \times 100 \tag{1.1}$$

2. *Total Harmonic Distortion (THD):* It is a very important factor to gauge the power quality of any system. Harmonic distortion is the degree to which a waveform deviates from its pure sinusoidal or fundamental values as a result of the summation of all these harmonic elements. So, the THD can be defined as the summation of all harmonic components of the voltage or current waveform compared against the fundamental

component of the voltage or current wave [14]. The equation (1.2) presents the mathematical formula of THD% in terms of the voltage waveform, where V_2, V_3, *and* V_n are the integer multiples of the voltage's fundamental frequency waveform (V_1). The steady-state output voltage distortion is also quantified with the THD. In case of a UPS system, a voltage source inverter with the *LC* filter is employed to provide the high frequency AC voltage waveforms. However, the finite output impedance caused by the *LC* filter and the dead-time effect of the inverter can distort the output voltage of the UPS system. Therefore, according to the IEEE Standard 519-1992, the UPS systems should provide THD within 3% and 5% for the linear and nonlinear loads, respectively [15]. Typically, the high performance UPS systems deliver a clean output voltage with a smaller THD values (i.e., below 2% for linear and 3% for nonlinear loads).

$$THD\% = \frac{\sqrt{V_2{}^2 + V_3{}^2 + \ldots + V_n{}^2}}{V_1} \times 100 = \frac{\sqrt{\sum_{n=2}^{\infty} V_n{}^2}}{V_1} \times 100 \qquad (1.2)$$

3. *Crest Factor (CF):* It is the ratio of the current waveform peak (I_{pk}) to rms value (I_{rms}) as depicted in (1.3). If an electrical signal (voltage or current) is a pure sinusoidal wave, the peak value for signal is 1.41 times the rms value. So, a linear load with a sinusoidal current waveform has a CF of $\sqrt{2}$ =1.41. An end-user that requires a nearly pure sine wave for signal analysis would want a source that could supply a near perfect sine wave with CF of 1.41. However, the reality is that most generated signals are not perfect in nature. Interactions between the supply and load (with all components in between) will cause distortions to signals and thus affect the relationship between the peak and rms values. Therefore for a nonlinear load, the CF value is greater than 1.41 and requires higher peak

currents due to the increased distortion at the output voltage. The optimal value for a crest factor depends upon the application. Normally, the CF of the nonlinear loads can be as high as 3, though in practice the CF on the UPS systems is unlikely to exceed 2.8 [16]. In conclusion, the CF value tells the end-user not only the purity of a signal but also the capability for a system to output a particular voltage or current. Besides that, it can be used in the absence of other data to realize the nonlinearity of load.

$$CF = \frac{I_{pk}}{I_{rms}} \tag{1.3}$$

In addition to the UPS steady-state performance criteria given above, the transient-state characteristic is also a determining factor of the UPS power quality. At transient-state, the sudden load disturbances in the linear load are a stimulating operating condition. In this case, the UPS performance is evaluated by the two criterions: voltage-dip (V_D) and settling time (S_t).

1. *Voltage-Dip (V_D):* According to the (1.4), the voltage dip is the percentage maximum output rms voltage deviation from its initial to the maximum sag point. In this equation, ΔV is the difference between the initial voltage (V_{ini}) and the voltage-dip point (V_{dp}). The Sudden load disturbances or transient can be a rapid rise or drop in load. For a high performance UPS system, the voltage dip should be less than 20% [17].

$$V_D\% = \frac{\Delta V}{V_{ini}} \times 100 = \frac{|V_{ini} - V_{dp}|}{|V_{ini}|} \times 100 \tag{1.4}$$

2. *Settling Time (S_t):* Similar to the voltage-dip, the settling time is also an important factor for the UPS transient-state performance. As described in (1.5), the settling time is the percentage deviation of total time during sudden load disturbances from starting of sag to steady-state voltage value. Where Δt is the difference between the initial time value t_{ini} and

the time at steady-state point t_{ssp}. If the duration of the sag is small, then the percentage voltage dip may not be too harmful to many loads involving energy storage elements (such as power supplies with diode rectifier front end involving large electrolytic capacitors in the DC-link). Thus, voltage dips larger than 20% may be tolerated provided that the time interval involved remains in several milliseconds [17].

$$St\% = \frac{\Delta t}{t_{ini}} \times 100 = \frac{|t_{ini} - t_{ssp}|}{|t_{ini}|} \times 100 \tag{1.5}$$

To attain a high UPS performance, it is very important to fulfill all of the abovementioned performance evaluation criteria within the standard values when subjected to any type of electrical loads. For this sake, the control approaches of the UPS inverter play a vital role. The subsequent section reviews the recently presented numerous control strategies to easily distinguish between their advantages and disadvantages.

1.3 Review of Existing Control Methods

Recently, many researchers have presented the following advanced control methods for the UPS inverter systems [18]-[33].

1. *Feedback Linearization Control Method:* The authors in [18] described a feedback linearization control scheme for the UPS inverter. This paper focuses on achieving the low THD and fast dynamic response without considering the parameters uncertainties.
2. *Repetitive Control Method*: In [19] and [20], a repetitive control technique is applied to generate a high-quality sinusoidal output voltage. In general, this technique has problems such as the slow transient response and the instability to error dynamics.
3. *Model Predictive Control Method*: In [21], a model predictive control approach is offered for regulating the UPS output voltage. This method

utilizes a load current observer and has a small steady-state error. However, it reflects a high THD value in the output voltage under linear and nonlinear loads.

4. *Hybrid PID Control Method:* In [22] and [23], two hybrid PID control schemes with multiple loops are proposed. With the advantages of ensuring a good performance and an easy implementation, these techniques require many trials to tune the proper gains.
5. *Deadbeat Control Method*: According to [24] and [25], a deadbeat control method can approve the fast dynamic response and high accuracy, but this scheme is very sensitive to the parameters uncertainties.
6. H_∞ *Loop–Shaping Control Method:* In [26], a H_∞ loop–shaping control scheme is presented. This method has a simple structure and is robust under model uncertainties. Nevertheless, it is applied to a single-phase inverter.
7. *Adaptive Fuzzy Control Method*: In [27], an adaptive fuzzy control technique is presented for a three-phase UPS system. Although this approach tracks the desired sinusoidal waveform regardless of being subjected to nonlinear load, the large number of fuzzy rules employed raises the computational burden.
8. *Hybrid Fuzzy-Repetitive Control Method:* In [28], a hybrid fuzzy-repetitive control approach is applied for the UPS inverter. This scheme reveals a good transient response under load disturbance; whereas it is applied to a single-phase UPS inverter and its THD value is high for nonlinear load.
9. *Sliding-Mode Control Method*: In [29]-[33], a sliding-mode control scheme is employed on the UPS inverter. It is obvious from [29]-[31] that good UPS performance can be obtained by this control scheme.

However, in [29], [30], the control scheme is only applied on a single-phase inverter and in [31] the results for the nonlinear load have not provided. In [32] and [33], the authors achieve a good voltage response, but the stability analysis is not presented.

1.4 Objectives and Composition of Thesis

In this thesis, an advanced control system for a three-phase UPS inverter is proposed to address and improve the issues that exist in the previous research works. To ensure the excellent UPS performance, the proposed control scheme combines the two artificial intelligent control laws, i.e., a fuzzy adaptive control law and a sliding-mode control law. The fuzzy adaptive law compensates the parameters uncertainties of the system being utilized as a compensation control term. While, the sliding-mode control law stabilizes the error dynamics of the system being employed as a feedback control term.

The main objectives of this thesis are:

- Propose an advance control system for a three-phase UPS inverter;
- Analyze the stability of the proposed control scheme;
- Verify the superior performance (such as fast dynamic response, small steady-state error, and low THD in the existence of the parameters uncertainties) of UPS system under various case-studies by providing the extensive simulation and experimental results in comparison with a conventional control scheme.

The remainder of the thesis is composed with the following chapters.

- Chapter 2 presents the mathematical modeling of the three-phase UPS inverter system including the three-phase UPS inverter with *LC* filter and space vector pulse width modulation (SVPWM).

- Chapter 3 discusses, first the overview of artificial intelligent control laws and second it illustrates the design and stability analysis of the proposed FASVC.
- Chapter 4 fully describes the comparative simulation and experimental results to validate the superior steady-state and transient-state performances of the proposed FASVC. Besides, it also presents the prototype setup of 1 kVA three-phase UPS inverter system.
- Chapter 5 addresses the conclusions and future work of this research work.

Chapter 2: Modeling of Three-Phase UPS Inverter System

This chapter presents the mathematical modeling of the three–phase UPS inverter system. First, the coordinate conversions in term of the Clarke and Park transformations with their inverses are described. After that, the modeling of a three-phase UPS inverter and space vector pulse width modulation (SVPWM) are derived successively.

2.1 Coordinate Transformations

For better analysis and easy computation of any three-phase power system, it is essential to convert it into a two-phase system. This projection is called as the coordinate transformation. In the following, the derivation of the most commonly used coordinate transformations named as Clarke and Park transformations along with their inverses are discussed [34], [35].

2.1.1 Clarke and Inverse Clarke Transformations

It is the transformation of a three-phase system (stationary *abc* reference frame) into the two-phase system (stationary *αβ* reference frame). Fig. 2-1 illustrates the Clarke transformation.

$$\begin{aligned} f_\alpha &= \frac{2}{3} f_a - \frac{1}{3}(f_b - f_c) \\ f_\beta &= \frac{2}{\sqrt{3}}(f_b - f_c) \\ f_0 &= \frac{1}{3}(f_a + f_b + f_c) \end{aligned} \tag{2.1}$$

where f_a,, f_b, f_c can be either phase current or phase voltage vectors of the

three-phase system. f_α, f_β are the components in the $\alpha\beta$ reference frame, f_0 is the homopolar component of the system. When f_α superposes with f_a, then the Clarke transformation is expressed by the following equation.

$$\begin{aligned} f_\alpha &= f_a \\ f_\beta &= \frac{1}{\sqrt{3}} f_a + \frac{1}{\sqrt{3}} f_b \\ f_a + f_b + f_c &= 0 \end{aligned} \tag{2.2}$$

The equation (2.2) can be rewritten in term of linear equation as:

$$\begin{bmatrix} f_\alpha \\ f_\beta \end{bmatrix} = \frac{2}{3} \begin{bmatrix} 1 & -1/2 & 1/2 \\ 0 & \sqrt{3}/2 & -\sqrt{3}/2 \end{bmatrix} \begin{bmatrix} f_a \\ f_b \\ f_c \end{bmatrix} \tag{2.3}$$

or

$$\begin{bmatrix} f_\alpha \\ f_\beta \end{bmatrix} = T_{abc \to \alpha\beta} \begin{bmatrix} f_a \\ f_b \\ f_c \end{bmatrix}$$

where

$$T_{abc \to \alpha\beta} = \frac{2}{3} \begin{bmatrix} 1 & -1/2 & 1/2 \\ 0 & \sqrt{3}/2 & -\sqrt{3}/2 \end{bmatrix} \tag{2.4}$$

In Fig. 2-1, the space vector $\bar{f}_s = f_\alpha + jf_\beta$ represents the original three-phase input signal in the stationary $\alpha\beta$ reference frame.

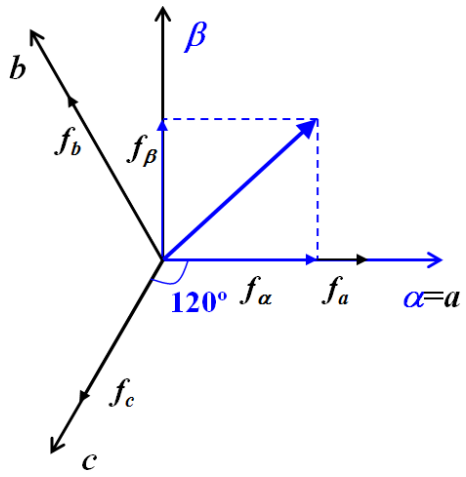

Fig. 2-1 Clarke transformation.

The modification from a two-phase system ($\alpha\beta$ reference frame) back into a three-phase system (abc) is called as inverse Clarke transformation and it can be expressed by the following equations:

$$\begin{aligned} f_a &= f_\alpha \\ f_b &= -\frac{1}{2} f_\alpha + \frac{\sqrt{3}}{2} f_\beta \\ f_c &= -\frac{1}{2} f_\alpha - \frac{\sqrt{3}}{2} f_\beta \end{aligned} \tag{2.5}$$

The equation (2.5) can be rewritten in term of linear equation as:

$$\begin{bmatrix} f_a \\ f_b \\ f_c \end{bmatrix} = \frac{1}{2} \begin{bmatrix} 2 & 0 \\ -1 & \sqrt{3} \\ -1 & -\sqrt{3} \end{bmatrix} \begin{bmatrix} f_\alpha \\ f_\beta \end{bmatrix} \tag{2.6}$$

or

$$\begin{bmatrix} f_a \\ f_b \\ f_c \end{bmatrix} = T_{\alpha\beta \to abc} \begin{bmatrix} f_\alpha \\ f_\beta \end{bmatrix}$$

where

$$T_{\alpha\beta\to abc} = \frac{1}{2}\begin{bmatrix} 2 & 0 \\ -1 & \sqrt{3} \\ -1 & -\sqrt{3} \end{bmatrix} \tag{2.7}$$

2.1.2 Park and Inverse Park Transformations

It is the transformation of the two orthogonal systems, in which the stationary $\alpha\beta$ reference frame is transformed into the synchronously rotating dq reference frame. Fig. 2-2 describes the Park transformation. The rotation of the dq over $\alpha\beta$ reference frame with an angle θ is done according to the following formulation:

$$\begin{aligned} f_d &= f_\alpha \cos\theta + f_\beta \sin\theta \\ f_q &= -f_\alpha \sin\theta + f_\beta \cos\theta \end{aligned} \tag{2.8}$$

The linear form of equation (2.8) can be written as

$$\begin{bmatrix} f_d \\ f_q \end{bmatrix} = \begin{bmatrix} \cos\theta & \sin\theta \\ -\sin\theta & \cos\theta \end{bmatrix} \begin{bmatrix} f_\alpha \\ f_\beta \end{bmatrix} \tag{2.9}$$

or

$$\begin{bmatrix} f_d \\ f_q \end{bmatrix} = T_{\alpha\beta\to dq} \begin{bmatrix} f_\alpha \\ f_\beta \end{bmatrix}$$

where

$$T_{\alpha\beta\to dq} = \begin{bmatrix} \cos\theta & \sin\theta \\ -\sin\theta & \cos\theta \end{bmatrix} \tag{2.10}$$

The angle θ can be defined in terms of angular frequency ω as

$$\theta = \omega.t$$

As shown in Fig. 2-2, the space vector $\bar{f}_s = f_d + jf_q$ represents the input signal in the synchronously rotating dq reference frame.

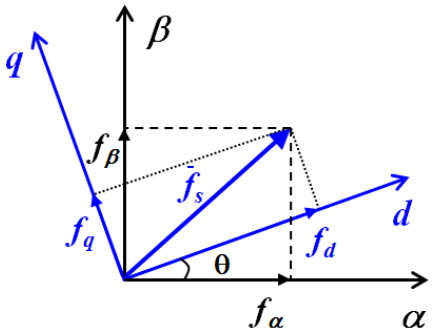

Fig. 2-2 Park transformation.

The conversion from the synchronously rotating *dq* reference frame back into stationary *αβ* reference frame is known as Inverse Park transformation and it can be calculated with a rotation over an angle θ according to the formulas:

$$\begin{aligned} f_\alpha &= f_d \cos\theta - f_q \sin\theta \\ f_\beta &= f_d \sin\theta + f_q \cos\theta \end{aligned} \tag{2.11}$$

The equation (2.11) can be rewritten in the matrix form as

$$\begin{bmatrix} f_\alpha \\ f_\beta \end{bmatrix} = \begin{bmatrix} \cos\theta & -\sin\theta \\ \sin\theta & \cos\theta \end{bmatrix} \begin{bmatrix} f_d \\ f_q \end{bmatrix} \tag{2.12}$$

or

$$\begin{bmatrix} f_\alpha \\ f_\beta \end{bmatrix} = T_{dq\to\alpha\beta} \begin{bmatrix} f_d \\ f_q \end{bmatrix}$$

where

$$T_{dq\to\alpha\beta} = \begin{bmatrix} \cos\theta & -\sin\theta \\ \sin\theta & \cos\theta \end{bmatrix} \tag{2.13}$$

2.2 System Modeling

In this section, the mathematical modeling of the three-phase UPS inverter system will be derived. This derivation is further divided into a

three-phase UPS inverter and a space vector pulse-width modulation. Fig. 2-3 illustrates the block diagram of UPS inverter system.

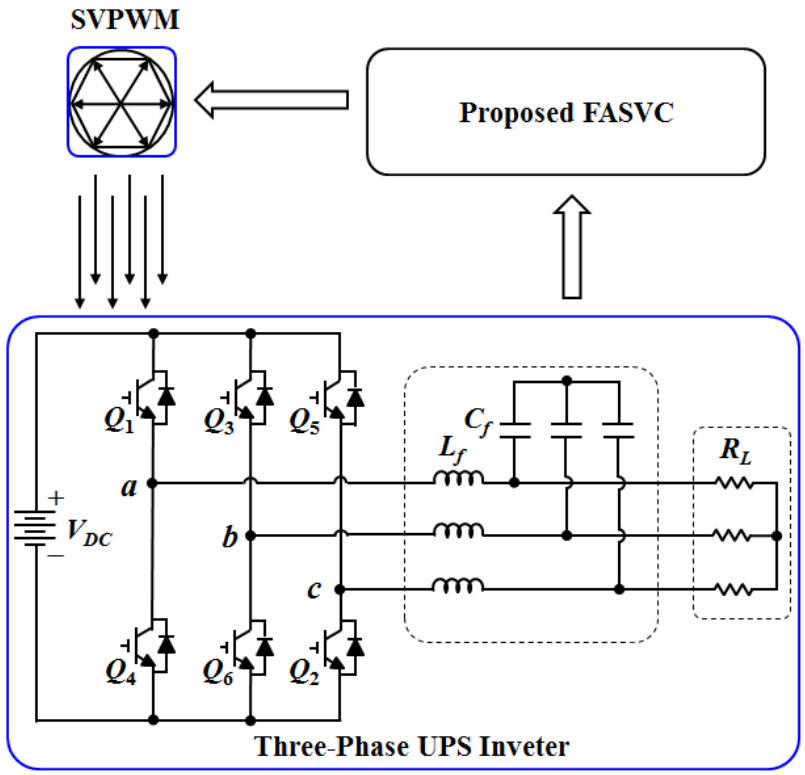

Fig. 2-3 Block diagram of a three-phase UPS inverter system.

2.2.1 Three-Phase UPS Inverter with *LC* Filter

In this research, the voltage source inverter (VSI) topology of a three-phase inverter with an *LC* output filter is used. The circuit diagram of the three-phase UPS inverter with an *LC* output filter is shown in Fig. 2-4. This figure consists of the following components: a DC-link (V_{DC}), six-IGBT power switches (Q_1-Q_6), three filter capacitors (C_f) and filter inductors (L_f), and a three-phase load (R_L). Furthermore, the quantities used in Fig. 2-4 are the load line to neutral voltages (v_{La}, v_{Lb}, v_{Lc}), load phase currents (i_{La}, i_{Lb}, i_{Lc}), inverter output line to neutral voltages (v_{ia}, v_{ib}, v_{ic}), inverter output phase

currents (i_{ia}, i_{ib}, i_{ic}), and capacitive phase currents (i_{fa}, i_{fb}, i_{fc}).

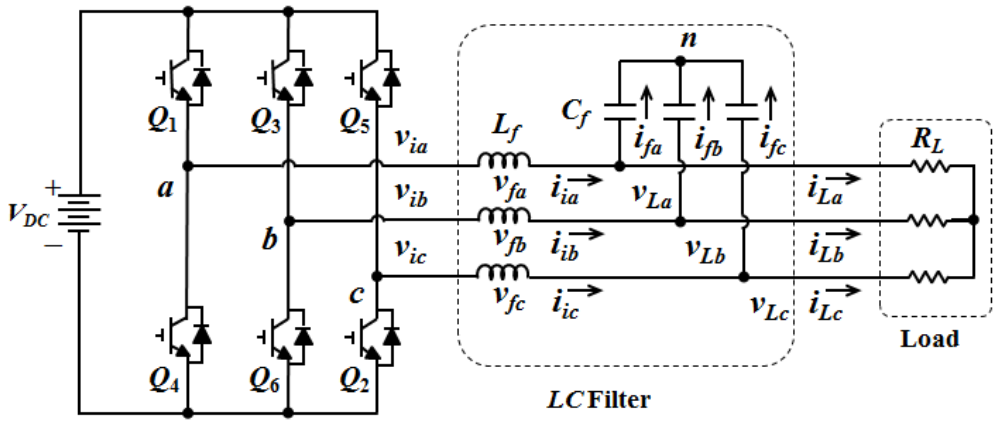

Fig. 2-4 Circuit diagram of a three-phase UPS inverter.

First, the state equations in stationary *abc* reference frame will be derived. Then, the *abc* model will be transformed into the *αβ* and *dq* reference frames by using the Clark (2.3) and Park transformations (2.9), respectively.

Let's apply the Kirchoff's current law (KCL) at nodes 1, 2, and 3, as shown in Fig. 2-5:

$$\begin{aligned} i_{ia} &= i_{fa} + i_{La} \\ i_{ia} &= C_f \frac{dv_{La}}{dt} + i_{La} \end{aligned} \tag{2.14}$$

$$\begin{aligned} i_{ib} &= i_{fb} + i_{Lb} \\ i_{ib} &= C_f \frac{dv_{Lb}}{dt} + i_{Lb} \end{aligned} \tag{2.15}$$

$$\begin{aligned} i_{ic} &= i_{fc} + i_{Lc} \\ i_{ic} &= C_f \frac{dv_{Lc}}{dt} + i_{Lc} \end{aligned} \tag{2.16}$$

or

$$\frac{dv_{La}}{dt} = \frac{1}{C_f} i_{ia} - \frac{1}{C_f} i_{La} \tag{2.17}$$

$$\frac{dv_{Lb}}{dt} = \frac{1}{C_f} i_{ib} - \frac{1}{C_f} i_{Lb} \tag{2.18}$$

$$\frac{dv_{Lc}}{dt} = \frac{1}{C_f} i_{ic} - \frac{1}{C_f} i_{Lc} \tag{2.19}$$

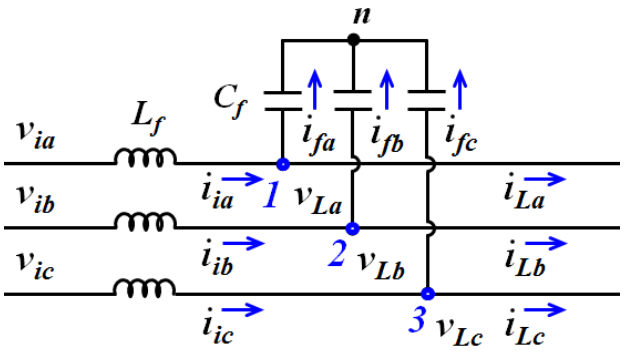

Fig. 2-5 Circuit diagram of KCL.

Now, apply Kirchoff's voltage law (KVL) to Loops 1, 2, and 3, as demonstrated in Fig. 2-6:

$$v_{ia} + v_{fa} + v_{La} = 0$$
$$v_{ia} + L_f \frac{di_{ia}}{dt} + v_{La} = 0 \tag{2.20}$$

$$v_{ib} + v_{fb} + v_{Lb} = 0$$
$$v_{ib} + L_f \frac{di_{ib}}{dt} + v_{Lb} = 0 \tag{2.21}$$

$$v_{ic} + v_{fc} + v_{Lc} = 0$$
$$v_{ic} + L_f \frac{di_{ic}}{dt} + v_{Lc} = 0 \tag{2.22}$$

or

$$\frac{di_{ia}}{dt} = \frac{1}{L_f} v_{ia} - \frac{1}{L_f} v_{La} \tag{2.23}$$

$$\frac{di_{ib}}{dt} = \frac{1}{L_f} v_{ib} - \frac{1}{L_f} v_{Lb} \tag{2.24}$$

$$\frac{di_{ic}}{dt} = \frac{1}{L_f} v_{ic} - \frac{1}{L_f} v_{Lc} \tag{2.25}$$

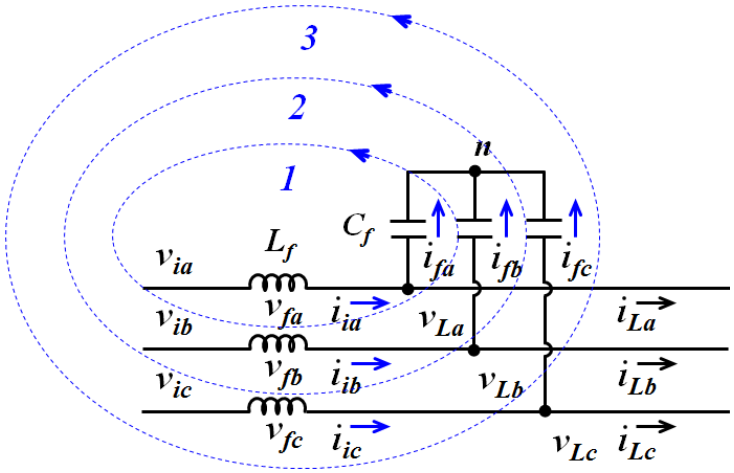

Fig. 2-6 Circuit diagram of KVL.

The equations (2.17)-(2.19) and (2.23)-(2.25) can be rewritten as:

$$\begin{aligned} \frac{d\mathbf{V}_{Labc}}{dt} &= \frac{1}{C_f}\mathbf{I}_{iabc} - \frac{1}{C_f}\mathbf{I}_{Labc} \\ \frac{d\mathbf{I}_{iabc}}{dt} &= \frac{1}{L_f}\mathbf{V}_{iabc} - \frac{1}{L_f}\mathbf{V}_{Labc} \end{aligned} \tag{2.26}$$

$$\mathbf{V}_{Labc} = \begin{bmatrix} v_{La} \\ v_{Lb} \\ v_{Lc} \end{bmatrix}, \quad \mathbf{I}_{Labc} = \begin{bmatrix} i_{La} \\ i_{Lb} \\ i_{Lc} \end{bmatrix}, \quad \mathbf{V}_{iabc} = \begin{bmatrix} v_{ia} \\ v_{ib} \\ v_{ic} \end{bmatrix}, \quad \mathbf{I}_{iabc} = \begin{bmatrix} i_{ia} \\ i_{ib} \\ i_{ic} \end{bmatrix}$$

where $\mathbf{V}_{Labc}$ and $\mathbf{I}_{Labc}$ are the load line to neutral voltage and current vectors, respectively, and $\mathbf{V}_{iabc}$ and $\mathbf{I}_{iabc}$ are the inverter output line to neutral voltage and current vectors, respectively, in the stationary *abc* reference frame.

Next, by using the Clark transformation (2.3), the above state equations (2.26) can be transformed to the stationary $\alpha\beta$ reference frame as

$$\begin{aligned} \frac{d\mathbf{V}_{L\alpha\beta}}{dt} &= \frac{1}{C_f}\mathbf{I}_{i\alpha\beta} - \frac{1}{C_f}\mathbf{I}_{L\alpha\beta} \\ \frac{d\mathbf{I}_{i\alpha\beta}}{dt} &= \frac{1}{L_f}\mathbf{V}_{i\alpha\beta} - \frac{1}{L_f}\mathbf{V}_{L\alpha\beta} \end{aligned} \tag{2.27}$$

$$\mathbf{V}_{L\alpha\beta} = \begin{bmatrix} v_{L\alpha} \\ v_{L\beta} \end{bmatrix}, \quad \mathbf{I}_{L\alpha\beta} = \begin{bmatrix} i_{L\alpha} \\ i_{L\beta} \end{bmatrix}, \quad \mathbf{V}_{i\alpha\beta} = \begin{bmatrix} v_{i\alpha} \\ v_{i\beta} \end{bmatrix}, \quad \mathbf{I}_{i\alpha\beta} = \begin{bmatrix} i_{i\alpha} \\ i_{i\beta} \end{bmatrix}$$

where $\mathbf{V}_{L\alpha\beta}$ and $\mathbf{I}_{L\alpha\beta}$ are the load line to neutral voltage and current vectors in the stationary $\alpha\beta$ reference frame, respectively. In addition, $\mathbf{V}_{i\alpha\beta}$ and $\mathbf{I}_{i\alpha\beta}$ are the inverter output line to neutral voltage and current vectors in the stationary $\alpha\beta$ reference frame, respectively.

After that, the following state equations in the synchronously rotating *dq* reference frame can be deduced by applying the Park transformation (2.9) on the (2.27):

$$\begin{aligned} \frac{d\mathbf{V}_{Ldq}}{dt} + j\omega\mathbf{V}_{Ldq} &= \frac{1}{C_f}\mathbf{I}_{idq} - \frac{1}{C_f}\mathbf{I}_{Ldq} \\ \frac{d\mathbf{I}_{idq}}{dt} + j\omega\mathbf{I}_{idq} &= \frac{1}{L_f}\mathbf{V}_{idq} - \frac{1}{L_f}\mathbf{V}_{Ldq} \end{aligned} \tag{2.28}$$

$$\mathbf{V}_{Ldq} = \begin{bmatrix} v_{Ld} \\ v_{Lq} \end{bmatrix}, \quad \mathbf{I}_{Ldq} = \begin{bmatrix} i_{Ld} \\ i_{Lq} \end{bmatrix}, \quad \mathbf{V}_{idq} = \begin{bmatrix} v_{id} \\ v_{iq} \end{bmatrix}, \quad \mathbf{I}_{idq} = \begin{bmatrix} i_{id} \\ i_{iq} \end{bmatrix}$$

where ω denotes the system angular frequency ($\omega = 2\pi f$), and f is the fundamental frequency of the load voltage. $\mathbf{V}_{Ldq}$ and $\mathbf{I}_{Ldq}$ are the load line to neutral voltage and current vectors in the synchronously rotating *dq* reference frame, respectively. Moreover, $\mathbf{V}_{idq}$ and $\mathbf{I}_{idq}$ are the inverter output

line to neutral voltage and current vectors in the synchronously rotating *dq* reference frame, respectively.

Finally, in order to get the desired state space model of the three-phase UPS inverter, the (2.28) can be rewritten in the following form:

$$\begin{aligned}
\dot{v}_{Ld} &= \omega v_{Lq} - \frac{1}{C_f} i_{Ld} + \frac{1}{C_f} i_{id} \\
\dot{v}_{Lq} &= -\omega v_{Ld} - \frac{1}{C_f} i_{Lq} + \frac{1}{C_f} i_{iq} \\
\dot{i}_{id} &= -\frac{1}{L_f} v_{Ld} + \omega i_{iq} + \frac{1}{L_f} v_{id} \\
\dot{i}_{iq} &= -\frac{1}{L_f} v_{Lq} - \omega i_{id} + \frac{1}{L_f} v_{iq}
\end{aligned} \tag{2.29}$$

where $\dot{v}_{Ld}$, $\dot{v}_{Lq}$, $\dot{i}_{id}$, and $\dot{i}_{iq}$ denote the time derivatives of v_{Ld}, v_{Lq}, i_{id}, and i_{iq}, respectively.

Now, the given plant model (2.29) can be expressed as the following continuous-time state space equation:

$$\dot{X}(t) = AX(t) + Bu(t) + Ed(t) \tag{2.30}$$

where

$$A = \begin{bmatrix} 0 & \omega & \frac{1}{C_f} & 0 \\ -\omega & 0 & 0 & \frac{1}{C_f} \\ -\frac{1}{L_f} & 0 & 0 & \omega \\ 0 & -\frac{1}{L_f} & -\omega & 0 \end{bmatrix}, \quad X(t) = \begin{bmatrix} v_{Ld} \\ v_{Lq} \\ i_{id} \\ i_{iq} \end{bmatrix},$$

$$B = \begin{bmatrix} 0 & 0 \\ 0 & 0 \\ \frac{1}{L_f} & 0 \\ 0 & \frac{1}{L_f} \end{bmatrix}, \quad u(t) = \begin{bmatrix} v_{id} \\ v_{iq} \end{bmatrix},$$

$$E = \begin{bmatrix} -\frac{1}{C_f} & 0 \\ 0 & -\frac{1}{C_f} \\ 0 & 0 \\ 0 & 0 \end{bmatrix}, \quad d(t) = \begin{bmatrix} i_{Ld} \\ i_{Lq} \end{bmatrix}$$

X(t), *u(t)*, and *d(t)* are the state variable, control input, and unknown disturbance, respectively, and *A*, *B*, and *E* are the constant matrices.

2.2.2 Space Vector Pulse Width Modulation (SVPWM)

Many types of the pulse-width modulation (PWM) schemes can be used for the switching of the six-IGBT power switches in the three-phase inverter. In this research, a space vector PWM technique (SVPWM) is chosen because of less harmonic distortion in the output voltages and more efficient use of supply voltage [36]. For realization of the SVPWM, a three-phase voltage or current vector in the *abc* reference frame is transformed into a vector in the stationary $\alpha\beta$ reference frame by employing the Clark transformation. Fig. 2-7 shows eight possible switching vectors of on and off patterns for the three upper IGBTs that feed the three-phase inverter. Six non-zero vectors (V_1-V_6) forms the axes of a hexagonal, and two zero vectors (V_0 and V_7) are at the origin. Also, the vectors divide the plane into six sectors, and the angle between any adjacent two non-zero vectors is 60º.

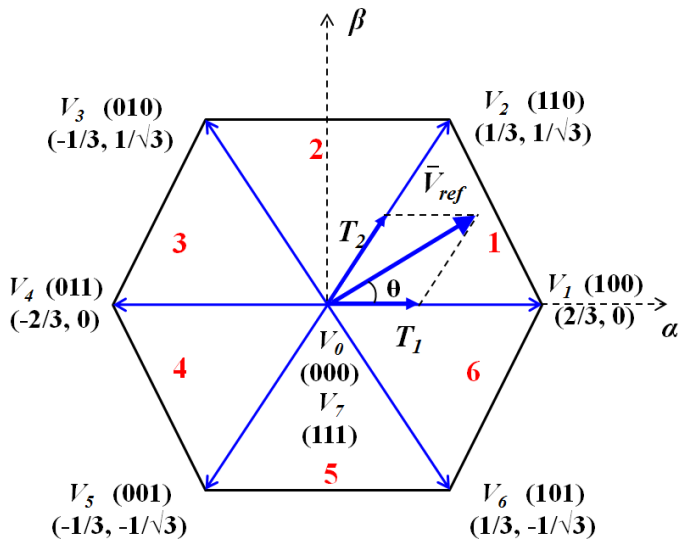

Fig. 2-7 Vector configuration of SVPWM with six sectors.

The SVPWM considers a complex voltage vector ($\overline{V}_{ref}$) as the reference signal to follow. This ($\overline{V}_{ref}$) is sampled with three switching durations (T_0, T_1, T_2) and the converter generates it by using a linear combination of possible state vectors. The modulation technique samples the reference signal and looks for the three nearest state vectors for determining their three duty cycles, respectively [37]. Hence, the output signal achieved by the converter is equal to the reference signal averaged over a sampling period. In order to illustrate the SVPWM method, the reference voltage vector ($\overline{V}_{ref}$) is generated with a linear combination of the three nearest vectors (100, 110 and 000 or 111) as shown in Fig. 2-8. In this figure, the sector 1 is selected for deriving the following equations (2.26) and (2.27).

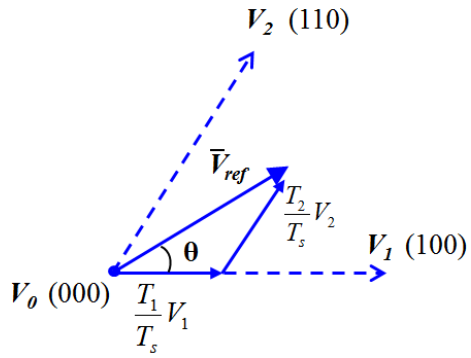

Fig. 2-8 Vector representations in sector 1.

$$\int_0^{T_S} \bar{V}_{ref} = \int_0^{T_1} V_1 dt + \int_T^{T_1+T_2} V_2 dt + \int_{T_1+T_2}^{T_S} V_0 \tag{2.31}$$

As we know

$$\begin{aligned} &T_S = T_0 + T_1 + T_2 \\ &\therefore T_S.V_{ref} = T_0.V_0 + T_1.V_1 + T_2.V_2 \\ &\Rightarrow T_S.|V_{ref}|.\begin{bmatrix}\cos\theta \\ \sin\theta\end{bmatrix} = 0 + T_1.\frac{2}{3}.V_{DC}.\begin{bmatrix}1 \\ 0\end{bmatrix} + T_2.\frac{2}{3}.V_{DC}.\begin{bmatrix}\cos \pi/3 \\ \sin \pi/3\end{bmatrix} \end{aligned} \tag{2.32}$$

where $0 \le \theta \le 60°$

Therefore, each switching time interval can be calculated as follows:

$$\begin{aligned} T_0 &= T_s - (T_1 + T_2), \\ T_1 &= T_s.k.\frac{(\sin \pi/3 - \theta)}{(\sin \pi/3)}, \\ T_2 &= T_s.k.\frac{(\sin \pi/3)}{(\sin \pi/3 - \theta)} \end{aligned} \tag{2.33}$$

where $k = \dfrac{|V_{ref}|}{2/3.V_{DC}}$.

Table I summarizes the switching time of the upper switches and the lower switches in a three-phase inverter.

TABLE I

SWITCHING TIME OF UPPER AND LOWER SWITCHES

Sector	Upper Switches (Q_1, Q_3, Q_5)	Lower Switches(Q_4, Q_6, Q_4)
1	$Q_1=T_1+T_2+T_{0/2}$ $Q_3=T_2+T_{0/2}$ $Q_5=T_{0/2}$	$Q_4=T_{0/2}$ $Q_6=T_2+T_{0/2}$ $Q_2=T_1+T_2+T_{0/2}$
2	$Q_1=T_1+T_{0/2}$ $Q_3=T_1+T_2+T_{0/2}$ $Q_5=T_{0/2}$	$Q_4=T_2+T_{0/2}$ $Q_6=T_{0/2}$ $Q_2=T_1+T_2+T_{0/2}$
3	$Q_1=T_{0/2}$ $Q_3=T_1+T_2+T_{0/2}$ $Q_5=T_2+T_{0/2}$	$Q_4=T_1+T_2+T_{0/2}$ $Q_6=T_{0/2}$ $Q_2=T_1+T_{0/2}$
4	$Q_1=T_{0/2}$ $Q_3=T_1+T_{0/2}$ $Q_5=T_1+T_2+T_{0/2}$	$Q_4=T_1+T_2+T_{0/2}$ $Q_6=T_2+T_{0/2}$ $Q_2=T_{0/2}$
5	$Q_1=T_2+T_{0/2}$ $Q_3=T_{0/2}$ $Q_5=T_1+T_2+T_{0/2}$	$Q_4=T_1+T_{0/2}$ $Q_6=T_1+T_2+T_{0/2}$ $Q_2=T_{0/2}$
6	$Q_1=T_1+T_2+T_{0/2}$ $Q_3=T_{0/2}$ $Q_5=T_1+T_{0/2}$	$Q_4=T_{0/2}$ $Q_6=T_1+T_2+T_{0/2}$ $Q_2=T_2+T_{0/2}$

2.3 Summary

In this chapter, the mathematical modeling of system (a three-phase UPS inverter system) was stated. This mathematical modeling included the detailed derivation of the coordinate transformations in term of the Clarke and Park transformations with their inverses, and the formation of the three-phase UPS inverter with *LC* filter and space vector pulse width modulation (SVPWM). This chapter provided a plant model for applying the proposed control system which will be designed in next chapter.

Chapter 3: Design and Stability Analysis of Proposed Fuzzy Adaptive Sliding-Mode Voltage Controller (FASVC)

This chapter deals with the design and stability analysis of the proposed control system (fuzzy adaptive sliding-mode voltage controller (FASVC)) for the three-phase UPS inverter system. First, an overview of the used control laws is described. Then, the design of the proposed FASVC including problem formulation, compensation control term, and feedback control term is presented. Finally, the stability of the proposed FASVC is analyzed by using Lyapunov functions.

3.1 Theoretical Background of Control Laws

This section illustrates the literature review of the control laws utilized in the proposed control system for the three-phase UPS inverter system.

The main factors which degrade the performance of the three-phase UPS inverter system are: the nonlinearity and uncertainties in terms of load type under normal or interruption conditions and parameters variations of *LC* filter which generally change in direct proportion to operation time, respectively. Thus, for achieving a perfect controllability of the three-phase UPS inverter system, it is significant to design such advance control system which not only provide solution to the nonlinearities and uncertainties of the system/plant, but also improves the stability of the whole system. On this note, the proposed control system accumulates the two artificial intelligent

control laws (such as a fuzzy adaptive control law and a sliding-mode control law) which are elaborated below.

3.1.1 Fuzzy Adaptive Control Law

In 1965, Lotfi A. Zadeh published his inspiring work "Fuzzy Sets", in which he described the mathematics of fuzzy set theory, and by extension fuzzy logic. A fuzzy logic controller (FLC) designed on the basis of the fuzzy logic, which allows us to emulate the human reasoning process in computers, quantify imprecise information, and make decision based on vague and incomplete data. The basic configuration of a FLC consists of a fuzzifier, fuzzy rule-base, a fuzzy inference engine, and a defuzzifier, as shown in Fig. 3-1. The fuzzifier is used to perform fuzzification (related to the vagueness and imprecision in a natural language) which translates the input crisp data into the fuzzy representation for further processing. A fuzzy system is characterized by a set of linguistic statements according to expert knowledge that is usually represented in the form of IF-THEN rules expressed as

IF *(a set of conditions are satisfied)*

THEN *(a set of consequences can be inferred)*

Moreover, to deal with the fuzzy information described above, the fuzzy inference engine employs to simulate human decision making based on the fuzzy IF-THEN rules in fuzzy rule base and the compositional rule of inference. Finally, the defuzzifier module is used to translate the processed fuzzy data into the crisp data suited to real world applications. This process is called as defuzzification.

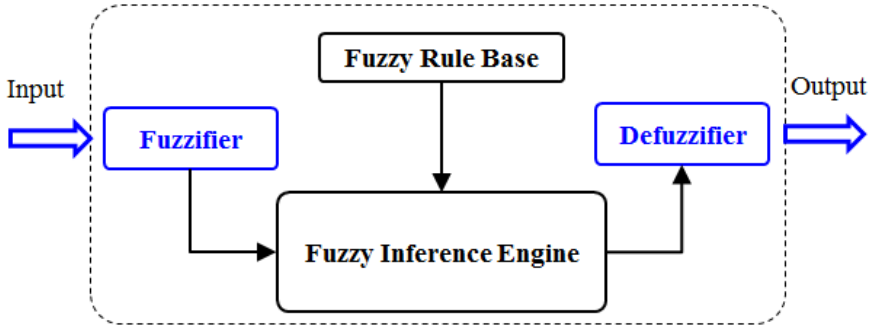

Fig. 3-1 Basic configuration of a FLC.

Despite the practical successes in many areas, the FLC seems to be deficient in formal analysis and robustness aspects. This is also a great resource of criticism from some control researchers. To overcome this drawback, in this research a fuzzy adaptive control law is utilized for achieving better control performance in the presence of any nonlinearities and uncertainties [38]-[40].

The main idea of fuzzy adaptive control system design is based on the universal approximation theorem [41], [42]. According to this theorem, a fuzzy model is first constructed to characterize the input/output behaviors of an uncertain system, then a controller for the uncertain system is designed, and the adaptive terms are determined to adjust the parameters of the fuzzy model. These adaptive terms are capable of approximating any real continuous function on a compact set to arbitrary accuracy.

3.1.2 Sliding-Mode Control Law

In control theory the sliding mode control is a form of variable structure control (VSC). In which the multiple control structures are designed so that trajectories always move toward a switching condition. Hence, the ultimate trajectory will slide along the boundaries of the control structures. The motion of the system is called a sliding mode [43], [44].

A surface $\sigma(x) = 0$ is attractive if:

- Any trajectory starting on the surface remains there;
- Any trajectory starting outside the surface tends to it at least asymptotically.

Thus, the conditions for a sliding motion are:

$$\lim_{\sigma \to 0^+} \dot{\sigma} < 0 \,, \qquad \lim_{\sigma \to 0^-} \dot{\sigma} > 0 \tag{3.1}$$

The above conditions ensure that the motion of the state trajectory x on either side of the switching surface $\sigma(x) = 0$ is toward the switching surface. Fig. 3-2 illustrates the sliding motion conditions. These conditions may be combined to give a reachability condition as

$$\sigma\dot{\sigma} < 0 \tag{3.2}$$

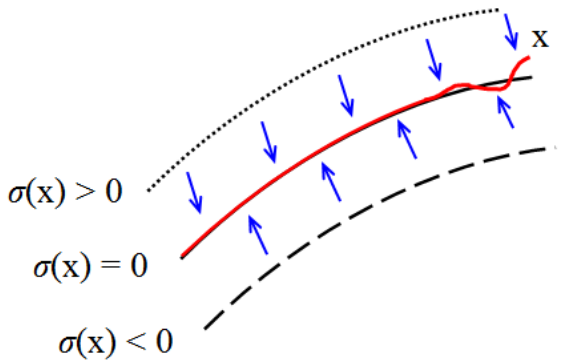

Fig. 3-2 Sliding motion conditions with attractiveness toward sliding surface.

3.2 Design of Proposed FASVC

Fig. 3-3 shows the diagram of proposed FASVC. The design of the proposed FASVC is combination of two control terms:

1. Compensation control term
2. Feedback control term

The former one adopts the fuzzy adaptive control law for solving the problems of the parameters uncertainties of the system. While the latter one employs the sliding-mode control law for stabilizing the error dynamics of the system.

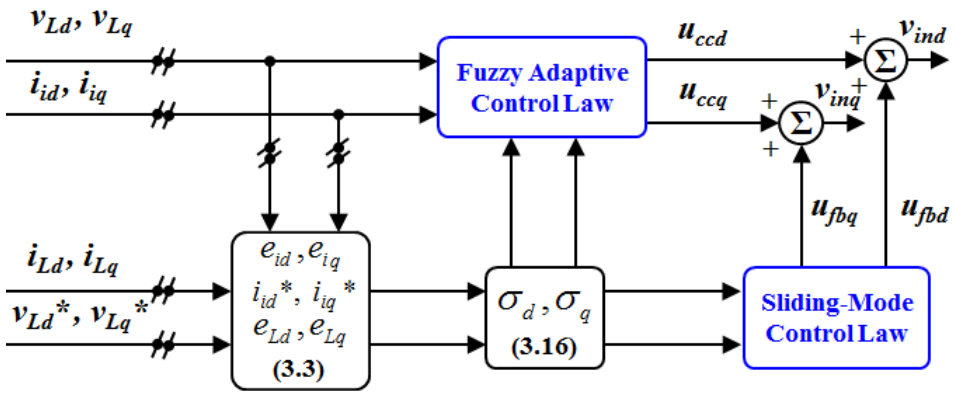

Fig. 3-3 Block diagram of the proposed FASVC.

3.2.1 Problem Formulation

By using the model of UPS inverter system (2.29),

$$\dot{v}_{Ld} = \omega v_{Lq} - \frac{1}{C_f} i_{Ld} + \frac{1}{C_f} i_{id}$$

$$\dot{v}_{Lq} = -\omega v_{Ld} - \frac{1}{C_f} i_{Lq} + \frac{1}{C_f} i_{iq}$$

$$\dot{i}_{id} = -\frac{1}{L_f} v_{Ld} + \omega i_{iq} + \frac{1}{L_f} v_{id}$$

$$\dot{i}_{iq} = -\frac{1}{L_f} v_{Lq} - \omega i_{id} + \frac{1}{L_f} v_{iq}$$

Let's consider the following assumptions:

- i_{id}, i_{iq} and v_{Ld}, v_{Lq} are the state variables and measurable;
- v_{id}, v_{iq} are the control inputs;

- i_{Ld}, i_{Lq} are the unknown disturbances and varies very slowly during the sampling period [19];
- The desired dq-axis load voltages (v_{Ld}*, v_{Lq}*) are constant during the sampling period and then their time derivatives can be set to be zero.

Now the errors of the dq-axis inverter currents (i_{id}, i_{iq}) and load voltages (v_{Ld}, v_{Lq}) can be defined as:

$$\begin{aligned} e_{id} &= i_{id} - i_{id}^*, \\ e_{iq} &= i_{iq} - i_{iq}^* \\ i_{id}^* &= i_{Ld} - \omega C_f v_{Lq}, \\ i_{iq}^* &= i_{Lq} + \omega C_f v_{Ld} \end{aligned} \tag{3.3}$$

$$\begin{aligned} e_{Ld} &= v_{Ld} - v_{Ld}^*, \\ e_{Lq} &= v_{Lq} - v_{Lq}^* \end{aligned} \tag{3.4}$$

where e_{id}, e_{iq} and i_{id}*, i_{iq}* are the errors and reference values of the dq-axis inverter currents, respectively, and i_{Ld}, i_{Lq} are the dq-axis load currents. Similarly, e_{Ld}, e_{Lq} and v_{Ld}*, v_{Lq}* are the errors and reference values of the dq-axis load voltages, respectively. Then, the following error dynamics can be derived:

$$\begin{aligned} \dot{e}_{id} &= -\frac{1}{L_f}(u_d - v_{ind}) + \frac{1}{\gamma_d}\frac{1}{C_f}e_{id} \\ \dot{e}_{iq} &= -\frac{1}{L_f}(u_q - v_{inq}) + \frac{1}{\gamma_q}\frac{1}{C_f}e_{iq} \\ \dot{e}_{Ld} &= \frac{1}{C_f}e_{id} \\ \dot{e}_{Lq} &= \frac{1}{C_f}e_{iq} \end{aligned} \tag{3.5}$$

where u_d, u_q and v_{ind} , v_{inq} are the system uncertainty terms and the control inputs, respectively, and γ_d, γ_q denote positive numbers.

Also, the system uncertainty terms (u_d, u_q) are given by

$$
\begin{aligned}
u_d &= -\frac{\omega L_f}{\gamma_d} v_{Lq} + \frac{L_f}{C_f \gamma_d} i_{Ld} - \frac{L_f}{C_f \gamma_d} i_{id} \\
&\quad - L_f \omega i_{iq} + L_f \dot{i}_{id}{}^* + v_{Ld}, \\
u_q &= \frac{\omega L_f}{\gamma_q} v_{Ld} + \frac{L_f}{C_f \gamma_q} i_{Lq} - \frac{L_f}{C_f \gamma_q} i_{iq} \\
&\quad + L_f \omega i_{id} + L_f \dot{i}_{iq}{}^* + v_{Lq}
\end{aligned}
\tag{3.6}
$$

It should be noticed from (3.6) that u_d and u_q contain the time derivative terms ($\dot{i}_{id}{}^*$, $\dot{i}_{iq}{}^*$) that cannot be computed straightforwardly due to the system noises. Besides, we assume that L_f has some uncertainties because of the nonlinear magnetic properties. Practically, the exact estimation of the uncertainty terms (u_d, u_q) is required instead of directly using the time derivatives of i_{id}* and i_{iq}*.

Next, the control inputs (v_{ind}, v_{inq}) can be written as

$$
\begin{aligned}
v_{ind} &= u_{ccd} + u_{fbd}, \\
v_{inq} &= u_{ccq} + u_{fbq}
\end{aligned}
\tag{3.7}
$$

where u_{ccd}, u_{ccq} and u_{fbd}, u_{fbq} are the dq-axis compensation control terms and the dq-axis feedback control terms, respectively.

3.2.2 Compensation Control Term

The compensation control terms (u_{ccd}, u_{ccq}) shown in (3.7) can be defined as

$$
\begin{aligned}
u_{ccd} &= u_d, \\
u_{ccq} &= u_q
\end{aligned}
\tag{3.8}
$$

Now (3.8) requires the accurate knowledge about u_d and u_q because of the parameters uncertainties. Thus, the following two fuzzy models η_d and η_q are applied to approximate u_d and u_q, respectively.

1. The i_{th} fuzzy rule of η_d:

IF x_1 is F_{1i} and x_2 is F_{2i} and x_3 is F_{3i} and x_4 is F_{4i}, THEN η_d is S_{di}.

2. The i_{th} fuzzy rule of η_q:

IF x_1 is F_{1i} and x_2 is F_{2i} and x_3 is F_{3i} and x_4 is F_{4i}, THEN η_q is S_{qi}.

where $i=1,2,\ldots, r,$ and r is the total number of fuzzy rules. $x_1=v_{Ld}$, $x_2=v_{Lq}$, $x_3=i_{id}$, $x_4=i_{iq}$. F_{ji} denote fuzzy sets associated with x_j. S_{di} and S_{qi} are the fuzzy singletons for η_d and η_q, respectively. The membership functions $g_{ji}(x_j)$ are used to further characterize the fuzzy sets F_{ji}. The final output (η_d, η_q) of the above fuzzy models can be inferred by using a standard fuzzy inference method that consists of a singleton fuzzifier, a product fuzzy inference, and a weighted average defuzzifier.

$$\begin{aligned} \eta_d &= \xi_d{}^T h = \sum_{i=1}^{r} \xi_{di} h_i, \\ \eta_q &= \xi_q{}^T h = \sum_{i=1}^{r} \xi_{qi} h_i \end{aligned} \tag{3.9}$$

where $\xi_d = [\xi_{d1}, \cdots, \xi_{dr}]^T$, $\xi_q = [\xi_{q1}, \cdots, \xi_{qr}]^T$ are the adjustable parameter vectors, and $h = [h_1, \cdots, h_r]^T$ is the fuzzy basis function. Moreover, the vector h_i is considered as a normalized weight of each IF-THEN rule, which satisfies $h_i \geq 0$ and $\sum_{i=1}^{r} h_i = 1$. Thus, h_i can be expressed as

$$h_i = \frac{\prod_{j=1}^{4} g_{ji}(x_j)}{\sum_{k=1}^{r} \prod_{j=1}^{4} g_{jk}(x_j)}, \quad i = 1,2,\ldots,r \tag{3.10}$$

Let's consider ξ_{*d} and ξ_{*q} are the optimal parameter vectors. According to the standard results of adaptive approximation [41], [42], a fuzzy system can uniformly approximate nonlinear functions to an arbitrary accuracy. So, if the searching spaces for η_d and η_q are sufficiently big, the following inequalities can be assumed

$$\varepsilon_d \geq |u_d - \eta_d| = |u_d - \xi_{*d}^T h|,$$
$$\varepsilon_q \geq |u_q - \eta_q| = |u_q - \xi_{*q}^T h| \tag{3.11}$$

Now, the compensation control terms (u_{ccd}, $u_{ccq)}$ can be written by:

$$u_{ccd} = \xi_d{}^T h = \sum_{i=1}^{r} \xi_{di} h_i,$$
$$u_{ccq} = \xi_q{}^T h = \sum_{i=1}^{r} \xi_{qi} h_i \tag{3.12}$$

$$\xi_{di} = -\frac{1}{\lambda_{di}} \int_0^t \sigma_d h_i dt,$$
$$\xi_{qi} = -\frac{1}{\lambda_{qi}} \int_0^t \sigma_q h_i dt \tag{3.13}$$

where σ_d, σ_q are the sliding surfaces and λ_{di}, λ_{qi} are positive design parameters.

The block diagram of the compensation control term is shown in Fig. 3-4.

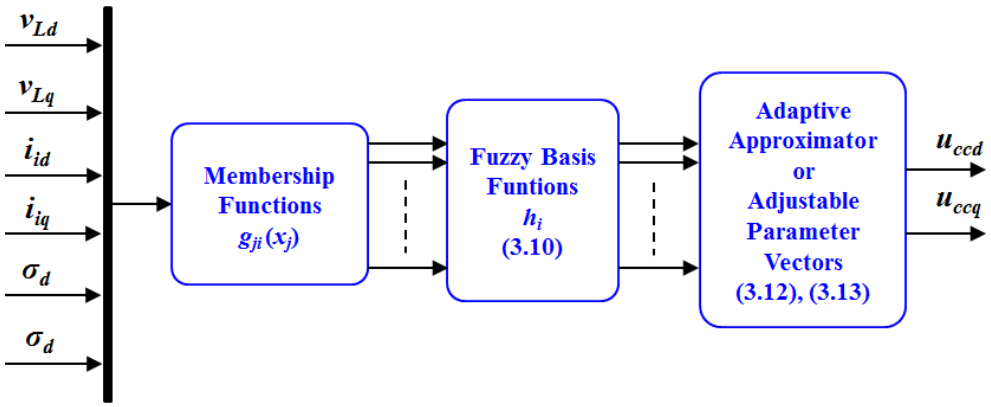

Fig. 3-4 Block diagram of the compensation control term.

3.2.3 Feedback Control Term

Fig. 3-5 presents the block diagram of the feedback control term. From the equation (3.7) the feedback control terms (u_{fbd}, u_{fbq}) can be clearly obtained as

$$u_{fbd} = -\tau_d \sigma_d - \varepsilon_d \text{sgn}(\sigma_d),$$
$$u_{fbq} = -\tau_q \sigma_q - \varepsilon_q \text{sgn}(\sigma_q) \quad (3.14)$$

$$\sigma_d = (e_{Ld} + \gamma_d e_{id}),$$
$$\sigma_q = (e_{Lq} + \gamma_q e_{iq}) \quad (3.15)$$

where σ_d, σ_q are the sliding surfaces , τ_d, τ_q, are the switching gains, ε_d, ε_q are the exponent coefficients. Also, τ_d, τ_q, ε_d, and ε_q are positive constants.

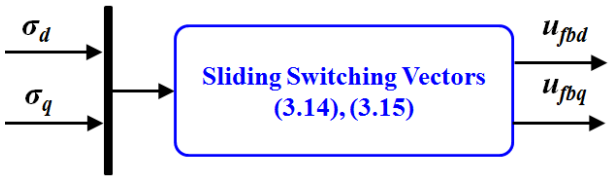

Fig. 3-5 Block diagram of the feedback control term.

3.3 Stability Analysis of Proposed FASVC

For better utilization of Lyapunov theory, first the stability of only feedback control term is analyzed. After that the combined stability of both control terms are proved.

Proposition 1: Assume that the filter capacitance C_f is known. Let the compensation control terms (u_{ccd}, u_{ccq}) and the feedback control terms (u_{fbd}, u_{fbq}) be obtained by the following control laws as:

$$u_{ccd} = \xi_d^{\,T} h = \sum_{i=1}^{r} \xi_{di} h_i,$$
$$u_{ccq} = \xi_q^{\,T} h = \sum_{i=1}^{r} \xi_{qi} h_i \quad (3.16)$$

$$u_{fbd} = -\tau_d \sigma_d - \varepsilon_d \text{sgn}(\sigma_d),$$
$$u_{fbq} = -\tau_q \sigma_q - \varepsilon_q \text{sgn}(\sigma_q) \quad (3.17)$$

Then e_{Ld} and $e_{Lq,}$ converge to zero.

Proof: The given control law (3.17) is known as a sliding-mode control law. Its stability analysis can be divided into two tasks. The first task is to

indicate the stability of the reduced-order sliding-mode dynamics while the second task is to verify the reachability condition. By setting $\dot{\sigma}_d = \sigma_d = \dot{\sigma}_q = \sigma_q = 0$, the second-order sliding-mode dynamics restricted to the sliding surface can be derived as

$$\begin{aligned} e_{Ld} + C_f \gamma_d \dot{e}_{Ld} &= 0, \\ e_{Lq} + C_f \gamma_q \dot{e}_{Lq} &= 0 \end{aligned}$$

which is asymptotically stable. Thus, it should be shown that the reachability condition is satisfied. To this end, the Lyapunov function $V_0(t)$ can be defined as

$$V_0(t) = \sigma_d^2 + \sigma_q^2 \tag{3.18}$$

Its time derivative is expressed as

$$\dot{V}_0 = 2(\sigma_d \dot{\sigma}_d + \sigma_q \dot{\sigma}_q) \tag{3.19}$$

Also, the following equation can be obtained from (3.5), (3.8), (3.14), and (3.15)

$$\begin{aligned} \dot{\sigma}_d &= \frac{\gamma_d}{L_f}(v_{ind} - u_d), \\ \dot{\sigma}_q &= \frac{\gamma_q}{L_f}(v_{inq} - u_q) \end{aligned} \tag{3.20}$$

Substituting (3.20) into (3.19) yields

$$\dot{V}_0 = -2\left(\tau_d \frac{\gamma_d}{L_f} \sigma_d^2 + \tau_q \frac{\gamma_q}{L_f} \sigma_q^2 \right) \leq 0 \tag{3.21}$$

Theorem 1: Assume that the filter capacitance C_f is known. And let the two control laws be given by (3.16) and (3.17). Then, e_{id}, e_{iq}, e_{Ld}, and e_{Lq} converge to zero and ξ_{di}, ξ_{qi} are bounded.

Proof: Since *Proposition 1* indicates that the linear sliding surface (3.15) guarantees the asymptotic stability of the sliding-mode dynamics, it should be demonstrated that σ_d, σ_q converge to zero. Let's define the Lyapunov function as

$$V(t) = \sigma_d^2 + \sigma_q^2 + \sum_{i=1}^{r} \frac{\gamma_d}{L_f} \lambda_{di} \tilde{\xi}_{di}^2 + \sum_{i=1}^{r} \frac{\gamma_q}{L_f} \lambda_{qi} \tilde{\xi}_{qi}^2 \tag{3.22}$$

where $\tilde{\xi}_{di} = \xi_{*di} - \xi_{di}$, $\tilde{\xi}_{qi} = \xi_{*qi} - \xi_{qi}$. Now the time derivative of (3.22) can be expressed as follows:

$$\dot{V} = 2(\sigma_d \dot{\sigma}_d + \sigma_q \dot{\sigma}_q - \sum_{i=1}^{r} \frac{\gamma_d}{L_f} \lambda_{di} \tilde{\xi}_{di} \dot{\xi}_{di} - \sum_{i=1}^{r} \frac{\gamma_q}{L_f} \lambda_{qi} \tilde{\xi}_{qi} \dot{\xi}_{qi}) \tag{3.23}$$

On the other hand, computation of (3.16) and (3.17) with (3.7) imply that

$$\begin{aligned} \nu_{ind} &= -\tau_d \sigma_d - \varepsilon_d \mathrm{sgn}(\sigma_d) + \xi_d^T h \pm \xi_{*d}^T h, \\ \nu_{inq} &= -\tau_q \sigma_q - \varepsilon_q \mathrm{sgn}(\sigma_q) + \xi_q^T h \pm \xi_{*q}^T h \end{aligned} \tag{3.24}$$

$$\begin{aligned} \dot{\xi}_{di} &= -\frac{1}{\lambda_{di}} h_i \sigma_d , \\ \dot{\xi}_{qi} &= -\frac{1}{\lambda_{qi}} h_i \sigma_q \end{aligned} \tag{3.25}$$

where $\dot{\xi}_{di}, \dot{\xi}_{qi}$ are the time derivatives adjustable/adaptive parameter vectors (ξ_{di}, ξ_{qi}). Also, the following equation can be derived from (3.5) and (3.24)

$$\begin{aligned} \dot{\sigma}_d &= \frac{\gamma_d}{L_f} [-\tau_d \sigma_d - \varepsilon_d \mathrm{sgn}(\sigma_d) + \tilde{\xi}_d^T h + (\xi_{*d}^T h - u_d)], \\ \dot{\sigma}_q &= \frac{\gamma_q}{L_f} [-\tau_q \sigma_q - \varepsilon_q \mathrm{sgn}(\sigma_q) + \tilde{\xi}_q^T h + (\xi_{*q}^T h - u_q)] \end{aligned} \tag{3.26}$$

If the inequalities in (3.11) are used, substitution of (3.24), (3.25) and (3.26) into (3.23) yields

$$\begin{aligned}\dot{V} &\le -2\frac{\gamma_d}{L_f}\left(\tau_d\sigma_d^2+\varepsilon_{\mathrm{d}}\,|\,\sigma_d\,|-(\xi_{*d}{}^T h-u_d)\sigma_d\right)\\ &\quad -2\frac{\gamma_q}{L_f}\left(\tau_q\sigma_q^2+\varepsilon_{\mathrm{q}}\,|\,\sigma_q\,|-(\xi_{*q}{}^T h-u_q)\sigma_q\right)\\ &\le -2\left(\tau_d\frac{\gamma_d}{L_f}\sigma_d^2+\tau_q\frac{\gamma_q}{L_f}\sigma_q^2\right)\le 0\end{aligned} \tag{3.27}$$

By applying the integration on both sides of (3.27):

$$\int_0^\infty \dot{V}(t)dt \le -2\left(\tau_d\frac{\gamma_d}{L_f}\int_0^\infty \sigma_d^2 dt+\tau_q\frac{\gamma_q}{L_f}\int_0^\infty \sigma_q^2 dt\right) \tag{3.28}$$

or

$$V(\infty)-V(0) \le -2\left(\tau_d\frac{\gamma_d}{L_f}\int_0^\infty \sigma_d^2 dt+\tau_q\frac{\gamma_q}{L_f}\int_0^\infty \sigma_q^2 dt\right) \tag{3.29}$$

Then, (3.29) can be redefined as

$$\begin{aligned}2\left(\tau_d\frac{\gamma_d}{L_f}\int_0^\infty \sigma_d^2 dt+\tau_q\frac{\gamma_q}{L_f}\int_0^\infty \sigma_q^2 dt\right) &\le V(0)-V(\infty)\\ &\le V(0)\end{aligned} \tag{3.30}$$

where $V_0(t) \ge 0$ is used. Then, the following inequalities can be derived:

$$\int_0^\infty \sigma_d^2 dt<\infty, \quad \int_0^\infty \sigma_q^2 dt<\infty \tag{3.31}$$

which implies that σ_d, $\sigma_q \in L_2$. Since $\dot{V} \le 0$ as shown in (3.27), $V(t)$ is nonincreasing and is upper bounded as $V(t) \le V(0)$. This entails that σ_d, $\sigma_q \in L_\infty$, and ξ_{di}, $\xi_{qi} \in L_\infty$. Hence, it can be concluded according to [42], [45], [46], and [47] that the closed-loop system is stable.

Now, the tuning method of controller gains and the estimation of load current values instead of using current sensors are explained by considering the following remarks.

Remark 3.1: This remark discusses the selection process of controller gains. In this research, for achieving the fast convergence and rapid transient

response, the adaptive gains (ξ_{di} and ξ_{qi}) are tuned to large values. According to (3.13), these adaptive gains are inversely proportional to λ_{di} and λ_{qi}, thus the smaller values of λ_{di} and λ_{qi} can result in the larger values of the adaptive gains and vice versa. On the contrary, the sliding surfaces (σ_d and σ_q) are further defined to obtain the feedback control terms (u_{fbd} and u_{fbq}) given in (3.14), (3.15), and these feedback control terms can be regarded as a PD controller. In this context, the control parameters γ_d, γ_q, τ_d, and τ_q can be designed based on the tuning rule of [48]. Finally, all control parameters/gains (γ_d, γ_q, τ_d, τ_q, λ_{di}, and λ_{qi}) can be tuned according to the following four steps:

1. Tune the parameters (γ_d, γ_q, τ_d, and τ_q) based on the tuning rule of [48];
2. Set quite large values for λ_{di} and λ_{qi};
3. Reduce λ_{di} and λ_{qi} by a small amount;
4. End the tuning process if the present control parameters give the satisfactory transient and steady-state performances; otherwise go back to *Step 3*.

The flow chart for the tuning rule is displayed in Fig 3-6.

Remark 3.2: As described in (16) and (17), the proposed FASVC consists of two control terms: a fuzzy adaptive compensation control term (u_{ccd}, u_{ccq}) and a sliding-mode feedback control term (u_{fbd} and u_{fbq}). The first one takes into account the parameter uncertainties. Meanwhile, the other one stabilizes the error dynamics of the system. Thus, the proposed control scheme can achieve a good performance in the existence of the parameter uncertainties.

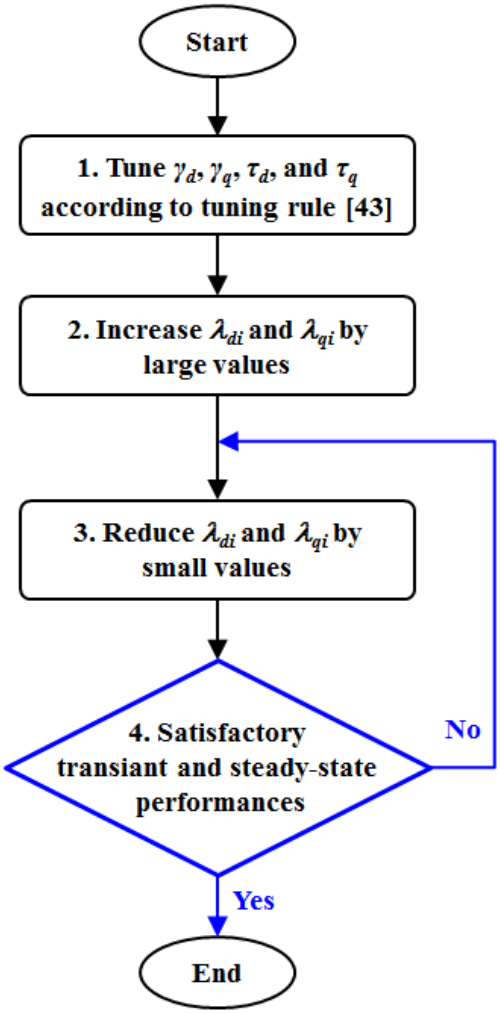

Fig. 3-6 Flow chart for tuning rule.

Remark 3.3: This remark reveals the estimation of the load currents through load current observer. The main reasons for employing the load current observer are to reduce the number of current sensors, decrease the system cost, and enhance the reliability of the overall system. In this research, a conventional load current observer named as Kalman-Bucy optimal observer is used [49]. Therefore, the load currents (i_{Ld}, i_{Lq}) in (3.3) are replaced with their estimated values (i_{estLd}, i_{estLq}), respectively. Fig. 3-7 describes the block diagram of the proposed FASVC with estimated load currents.

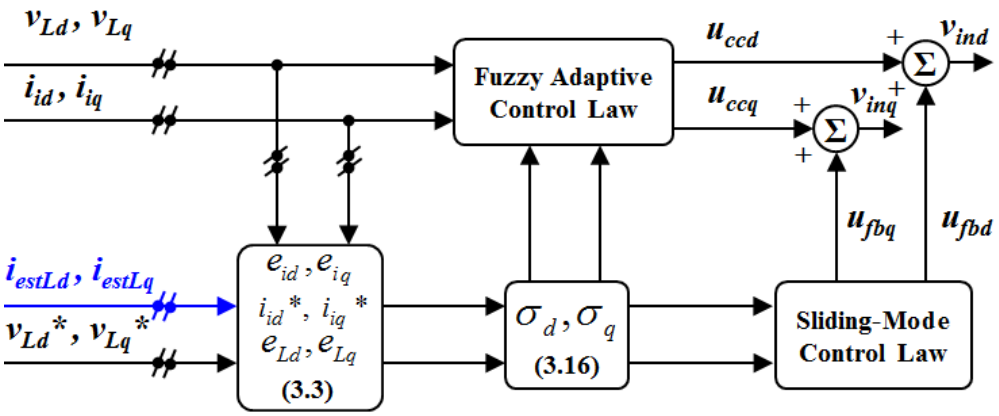

Fig. 3-7 Block diagram of the proposed FASVC with estimated load currents.

3.4 Summary

In this chapter, the design of the proposed fuzzy adaptive sliding-mode voltage controller (FASVC) for the three-phase UPS inverter system was demonstrated. First, the used artificial intelligent control laws were reviewed. Second, the proposed FASVC including problem formulation, compensation control term, and feedback control term was developed. Next, the stability of the proposed FASVC was analyzed by employing the Lyapunov functions. In short, this chapter provided a complete design of the proposed control system to be simulated and tested in the next chapter with the laboratory prototype setup.

Chapter 4: Performance Validations through Comparative Simulation and Experimental Results

This chapter validates the excellent performance of the proposed FASVC under case-studies through comparative simulation and experimental results. First, the prototype setup of whole three-phase UPS inverter system is presented. Next, the selection of the performance indices, such as membership functions, controller gains, parameters uncertainties, and case-studies, are described in detail. Finally, the comparative simulation and experimental results of the proposed FASVC as well as conventional SMC are illustrated to clarify the superior performance of the proposed control system.

4.1 Prototype Setup

In this section, in order to verify the effectiveness of the proposed control system, a laboratory test-bed of a 1 kVA three-phase UPS inverter system is developed and implemented as portrayed in Fig. 4-1. The components used in the laboratory test-bed are stated below:

- A three-leg six-IGBT power converter manufactured by SEMIKRON, as three-phase UPS inverter;
- LV-25P voltage sensors and LTS-6NP current sensors manufactured by LEM, installed for measuring the feedback voltage and current signals;
- Analog to digital converters, employed to digitize the measured signals;

- A 32-bit floating point TMS320F28335 digital signal processor (DSP) manufactured by TEXAS INSTRUMENTS, for executing the software/code.

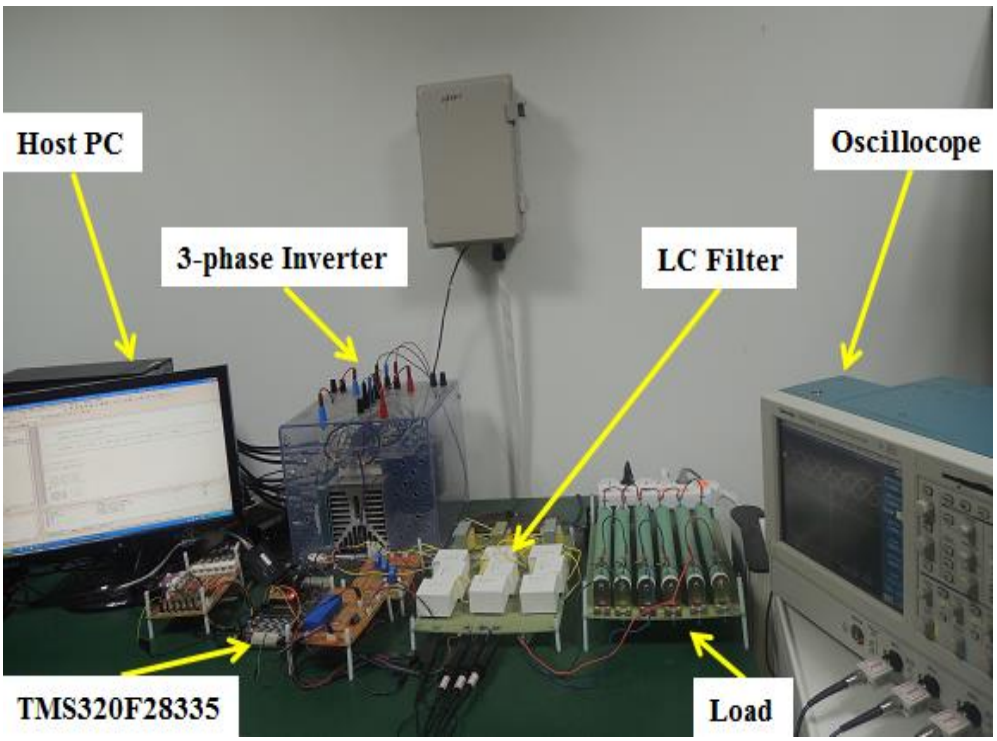

Fig. 4-2 Laboratory test-bed of a 1 kVA three-phase UPS inverter system.

The performance investigations are carried using the simulation results obtained from MATLAB/Simulink software and the experimental results obtained on the developed prototype with a TMS320F28335 DSP.

Table II summarizes the specifications of the three-phase UPS inverter. Note that the values of the *LC* output filter have a cutoff frequency of 620 Hz. Generally, larger values of the filter elements (L_f and C_f) can realize the better filter performance. On the other hand, the large values of L_f and C_f can increase the system cost and volume. Also, a large current flows into C_f even at no load. Hence, to select the *LC* filter parameters, one should always

follow a trade-off between their advantages and disadvantages. More details (i.e., guidelines of choosing the *LC* values) about how the output filter parameters can be determined for the pulse width modulation inverters are available in [50].

TABLE II

PARAMETERS OF A THREE-PHASE UPS INVERTER

Parameters	**Values**
Rated power	1 kVA
Fundamental frequency f	60 Hz
Load output voltages $V_{Labc,\,rms}$	110 V
Switching frequency	5 kHz
Output filter capacitance C_f	6.5 μF
Output filter inductance L_f	10 mH
Sampling time	200 μs
DC-link voltage V_{DC}	295 V

The complete circuit configuration of the three-phase inverter system is shown in Fig. 4-2. In this figure, both the inverter currents ($\mathbf{I}_{iabc}$) and load voltages ($\mathbf{V}_{Labc}$) in the stationary *abc* reference frame are sensed, and then simultaneously transformed to the values in the stationary $\alpha\beta$ reference frame ($\mathbf{V}_{L\alpha\beta}$, $\mathbf{I}_{i\alpha\beta}$) and synchronously rotating *dq* reference frame ($\mathbf{V}_{Ldq}$, $\mathbf{I}_{idq}$) by using Clarke's and Park's transformations, respectively. These values are first used at the conventional load current observer. After that, the estimated load currents (i_{estLd}, i_{estLq}) as well as the reference load voltages (v_{Ld}*, v_{Lq}*) are injected in the proposed FASVC. Thereafter the *dq*-axis voltage control inputs (v_{ind}, v_{inq}) are converted to the quantities ($v_{in\alpha}$, $v_{in\beta}$) in the stationary $\alpha\beta$ reference frame using an inverse Park's transformation, six gate pulses are

generated to drive the three-phase UPS inverter by using space vector pulse-width modulation (SVPWM) technique with the sampling time of 200μs and switching frequency of 5 kHz.

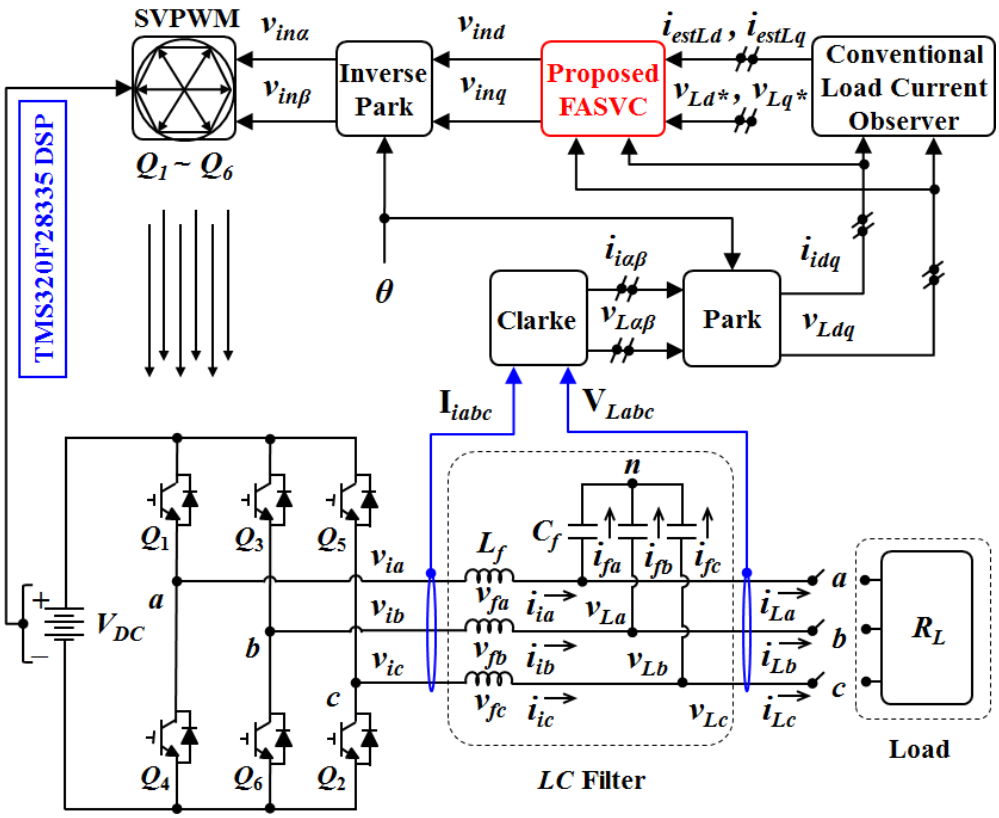

Fig. 4-2 Overall block diagram of a 1 kVA three-phase UPS inverter system.

4.2 Performance Indices

4.2.1 Fuzzy Rules and Controller Gains

In order to create the fuzzy models η_d and η_q given in (16), the total numbers of fuzzy rules for four state variables (v_{Ld}, v_{Lq}, i_{id}, and i_{iq}) are optimized as

$$r = (F)^m = (2)^4 = 16$$

where F donates the fuzzy sets and m is the number of state variables

In this research, the fuzzy sets are characterized by two linguistic terms (negative *N* and positive *P*) for each state variable and designed in the form of the membership functions. Because of the simplicity and easy implementation, the Gaussian functions are adopted as the membership functions. The formula for the Gaussian function can be found in [51]:

$$g(x, \psi) = e^{-(x \pm \psi)^2 / (2\psi)^2} \tag{4.1}$$

where x and ψ denote the input/state variable and constant parameter of the Guassian function, respectively.

Now, based on equation (4.1) the following functions can be formed:

$$g_{N1}(v_{Ld}, 160) = e^{-(v_{Ld}+160)^2/(320)^2},\ g_{P1}(v_{Ld}, 160) = e^{-(v_{Ld}-160)^2/(320)^2}$$

$$g_{N2}(v_{Lq}, 5) = e^{-(v_{Lq}+5)^2/(10)^2},\ g_{P2}(v_{Lq}, 5) = e^{-(v_{Lq}-5)^2/(10)^2}$$

$$g_{N3}(i_{id}, 6) = e^{-(i_{id}+6)^2/(12)^2},\ g_{P3}(i_{id}, 6) = e^{-(i_{id}-6)^2/(12)^2}$$

$$g_{N4}(i_{iq}, 2) = e^{-(i_{iq}+2)^2/(4)^2},\ g_{P4}(i_{iq}, 2) = e^{-(i_{iq}-2)^2/4)^2}.$$

where 160, 5, 6, and 2 are the constant values which are respectively chosen by considering the constraints of each state variable with a small additional tolerance. Fig 4-3 displays the shapes of the chosen Gaussian functions.

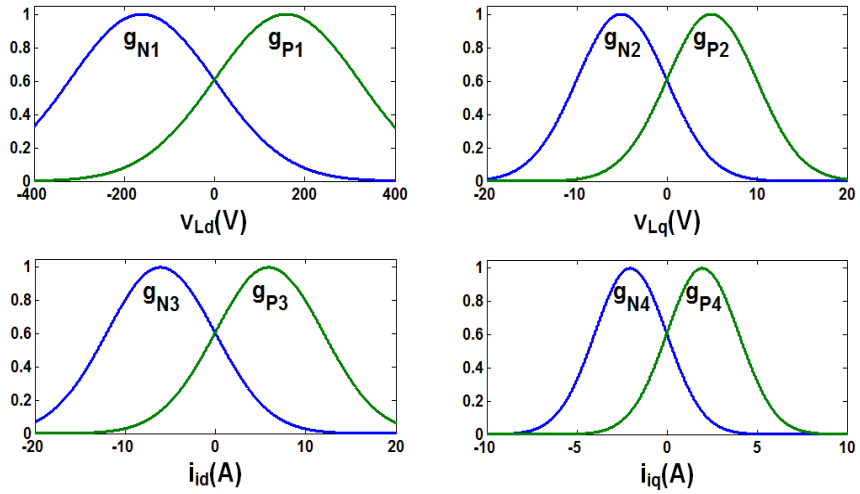

Fig. 4-3 Graphical representation of Gaussian functions.

More briefly, the sixteen fuzzy rules for each fuzzy model (η_d and η_q) can be, simultaneously, represented as

- Fuzzy rule 1 for η_d: IF v_{Ld} is N_1 and v_{Lq} is N_2 and i_{Ld} is N_3 and i_{Lq} is N_4, THEN η_d is ξ_{d1}.
- Fuzzy rule 2 for η_d: IF v_{Ld} is N_1 and v_{Lq} is N_2 and i_{Ld} is N_3 and i_{Lq} is P_4, THEN η_d is ξ_{d2}.
- Fuzzy rule 3 for η_d: IF v_{Ld} is N_1 and v_{Lq} is N_2 and i_{Ld} is P_3 and i_{Lq} is N_4, THEN η_d is ξ_{d3}.

.
.
.

- Fuzzy rule 16 for η_d: IF v_{Ld} is P_1 and v_{Lq} is P_2 and i_{Ld} is P_3 and i_{Lq} is P_4, THEN η_d is ξ_{d16}.

and

- Fuzzy rule 1 for η_q: IF v_{Ld} is N_1 and v_{Lq} is N_2 and i_{Ld} is N_3 and i_{Lq} is N_4, THEN η_q is ξ_{q1}.
- Fuzzy rule 2 for η_q: IF v_{Ld} is N_1 and v_{Lq} is N_2 and i_{Ld} is N_3 and i_{Lq} is P_4,

THEN η_q is ξ_{q2}.

- Fuzzy rule 3 for η_q: IF v_{Ld} is N_1 and v_{Lq} is N_2 and i_{Ld} is P_3 and i_{Lq} is N_4, THEN η_q is ξ_{q3}.

.
.
.

- Fuzzy rule 16 for η_q: IF v_{Ld} is P_1 and v_{Lq} is P_2 and i_{Ld} is P_3 and i_{Lq} is P_4, THEN η_q is ξ_{q16}.

Finally, after extensive simulation studies, the controller gains are selected according to the tuning rule mentioned in *Remark 3.1*:

$$\gamma_d = \gamma_q = 130$$
$$\tau_d = \tau_q = 15$$
$$\varepsilon_d = \varepsilon_q = 70$$
$$\lambda_{di} = \lambda_{qi} = 55\text{x}10^{-5}$$

4.2.2 Parameters Uncertainties

The robustness or insensitivity against system parameters uncertainties is an important indicator of high performance for any control system.

In case of designing a new controller for the UPS inverter system, the parameters uncertainties of the output *LC* filter are very crucial. Because, in practical applications the working capability of the inductor and capacitor can deteriorate as time passes. The key factors behind this degradation are the variation in the capacitor's dielectric properties and saturation in the inductor's magnetic core depending upon their parasite resistance and temperature [52]. Thus in this research, the parameter variation of the *LC* output filter are realized by their 30% reduction.

$$L_f = (100\%–30\%)\times 10 = 7.0 \text{ mH},$$
$$C_f = (100\%–30\%)\times 6.5 = 4.4 \text{ μF}.$$

4.2.3 Case-Studies

To effectively demonstrate the steady-state and transient-state performances of the proposed FASVC, both the simulation and experiment are performed under three different case-studies: sudden load disturbances, sudden unbalanced load, and nonlinear load. Table III presents the values of elements used in each case-study.

TABLE III

VALUES OF LOAD ELEMENTS

Case-Studies	Load Conditions	Elements	Values
1	Sudden load disturbances	Resistor R_L	40 Ω
2	Sudden Unbalanced Load	Resistor R_L	40 Ω
3	Nonlinear Load	Resistor R_{LN}	90 Ω
		Inductor L_{LN}	10 mH
		Capacitor C_{LN}	60 μF

Case 1. *Sudden load disturbances*: The balanced resistive load is instantaneously applied to the inverter output terminals from full load to no-load and vice versa, i.e., (100%−0%−100%), as shown in Fig. 4-4(a).

Case 2. *Sudden Unbalanced load*: The unbalanced resistive load is abruptly connected to the inverter output terminals, i.e., only phase *c* is opened, as portrayed in Fig. 4-4(b).

Case 3. *Nonlinear load*: A three-phase full-bridge diode rectifier is connected to the inverter output terminals. It is also connected in parallel with an inductor (L_{LN}), a capacitor (C_{LN}), and a resistor (R_{LN}), as displayed in Fig. 4-4(c). Moreover, the crest factor of 1.62 is measured for this nonlinear load.

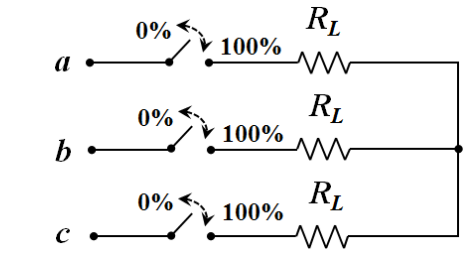

(a)

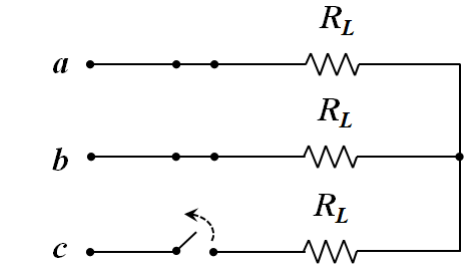

(b)

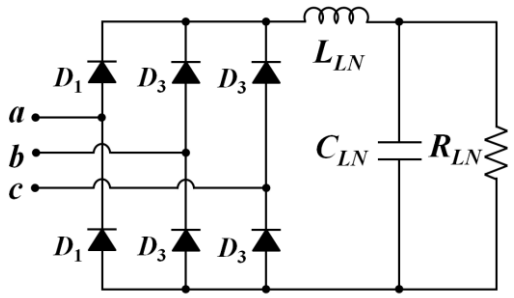

(c)

Fig. 4-4 Circuit diagrams of loads for three case-studies. (a) Sudden load disturbances (100%−0%−100%). (b) Sudden unbalanced load (Phase *c* open). (c) Nonlinear load (A three-phase *RLC* diode rectifier)

4.3 Comparative Simulation Results

In this section, the simulation results of the proposed FASVC as well as the conventional SMC are demonstrated. According to the chosen case-studies, these results are divided into three subsections in which the performance of the proposed FASVC and the conventional SMC is described by considering the −30% parameters uncertainties for each case-study. Furthermore, every figure expresses the waveforms of the load voltages ($\mathbf{V}_{Labc}$), inverter currents ($\mathbf{I}_{iabc}$), load currents ($\mathbf{I}_{Labc}$), estimated load currents ($\mathbf{I}_{estLabc}$), and phase *a* load current error ($e_{La}=i_{La}-i_{estLa}$).

4.3.1 Case 1: Sudden Load Disturbances

Fig. 4-5 presents the simulation results of the proposed FASC and conventional SMC scheme, when a balanced resistive load is suddenly applied at the instant of 0.121 s and 0.15 s to the inverter output terminals from full load to no-load and vice versa, i.e., (100%−0%−100%). In detail, Figs. 4-5(a) shows that the load voltage waveforms ($\mathbf{V}_{Labc}$) are slightly distorted with a voltage-dip (38 V) and recovered to the steady-state within 0.5 ms. On the other hand, Fig. 4-5(b) shows that it takes 1.0 ms for the $\mathbf{V}_{Labc}$ to be resumed to its pre-disturbance steady-state value. Thus, it is depicted that the proposed FASVC accomplishes a smaller voltage-dip in a shorter settling time as compared to the conventional SMC, i.e., (38 V / 57 V and 0.5 ms / 1.0 ms).

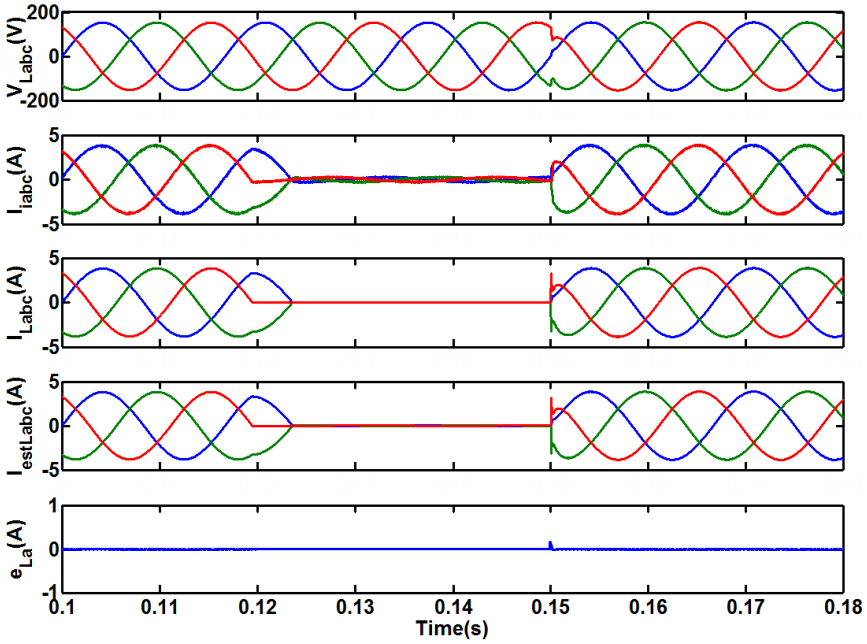

(a)

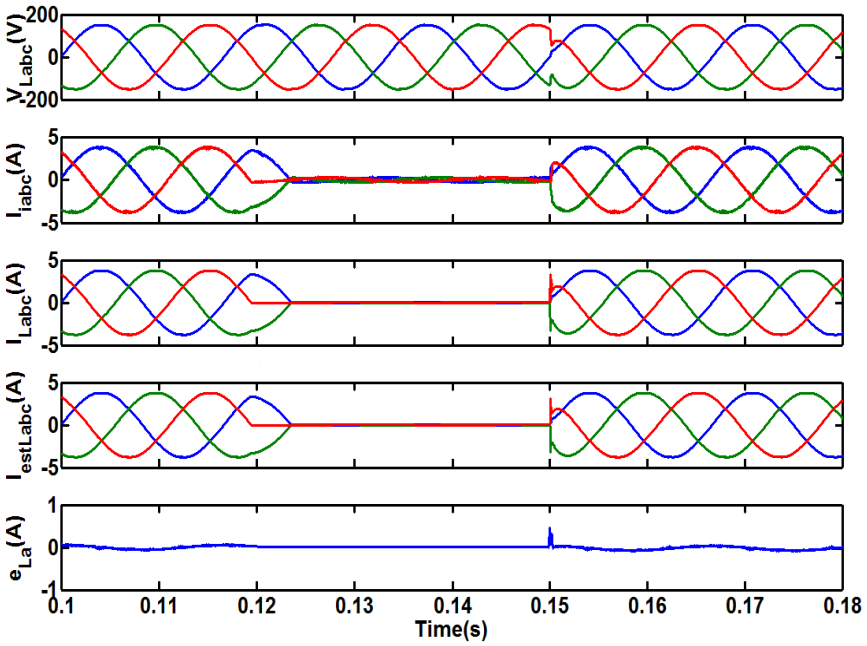

(b)

Fig. 4-5 Comparative simulation results under sudden load disturbances with –30% parameters uncertainties in L_f and C_f. (a) Proposed FASVC. (b) Conventional SMC.

4.3.2 Case 2: Sudden Unbalanced Load

Fig. 4-6 describes the comparative simulation results, when an unbalanced resistive load is suddenly connected to the inverter output terminals at t = 0.136 s, i.e., only phase *c* is opened. More specifically, the load voltage waveforms ($\mathbf{V}_{Labc}$) of the proposed FASVC presented in Fig. 4-6(a) looks quite sinusoidal compare with the conventional SMC shown in Fig. 4-6(b). Furthermore, the proposed FASVC exhibits a lower THD value and a slighter steady-state error than the conventional SMC, i.e., (0.35% / 0.81% and 0.09% / 1.27%).

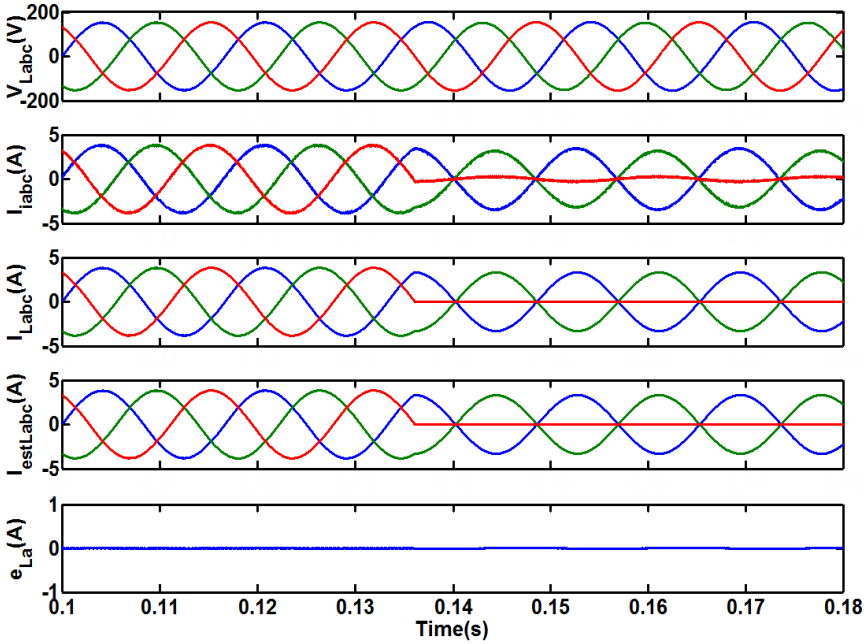

(a)

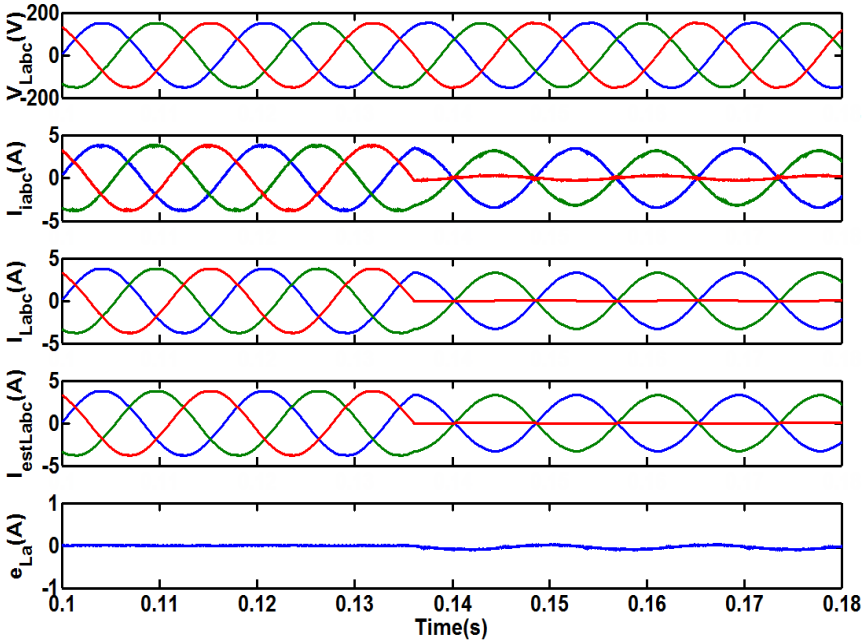

(b)

Fig. 4-6 Comparative simulation results under unbalanced load with –30% parameters uncertainties in L_f and C_f. (a) Proposed FASVC. (b) Conventional SMC.

4.3.3 Case 3: Nonlinear Load

Fig. 4-7 illustrates the simulation results of the proposed FASC and conventional SMC, when a nonlinear load of a three-phase full-bridge diode rectifier with parallel *RLC* elements is connected to the inverter output terminals. Examining the load voltage waveforms ($\mathbf{V}_{Labc}$) of the proposed FASVC given in Fig. 4-7(a), it can revealed that a pure sinusoidal behavior than the conventional SMC displayed in Fig. 4-7(b). Moreover the proposed FASVC achieves a THD of 1.02% and a steady-state error of 0.40%, which are respectively smaller as compared to the conventional SMC, i.e., (2.80% and 2.15%).

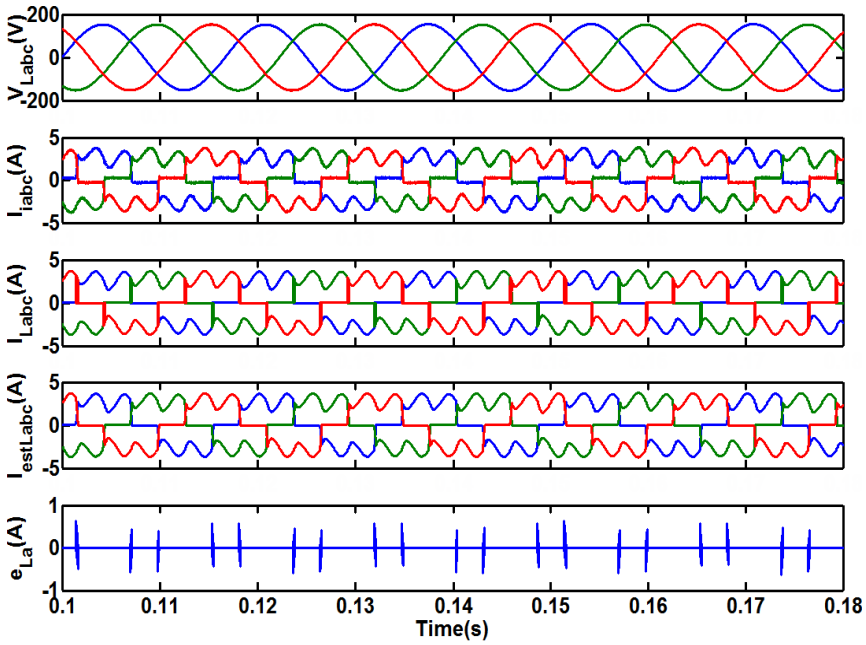

(a)

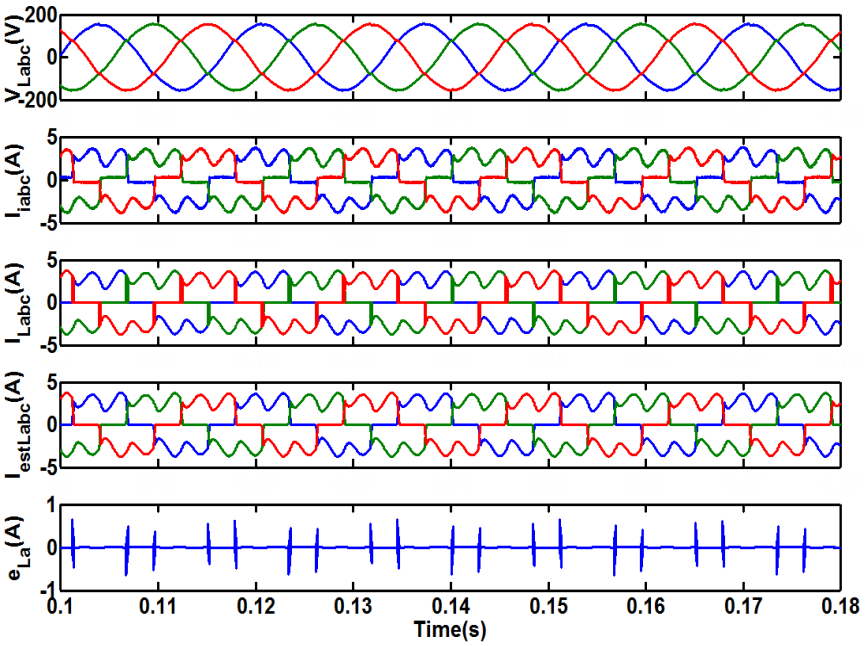

(b)

Fig. 4-7 Comparative simulation results under nonlinear load with –30% parameters uncertainties in L_f and C_f. (a) Proposed FASVC. (b) Conventional SMC.

Table IV summarizes the comparative simulation results between the proposed FASVC and the conventional SMC applied for voltage regulation during the steady-state and transient-state. According to Table IV, at steady-state both the THDs and the steady-state errors of the proposed FASVC results in a reasonable improvement (within 1.1% and 0.5%) as compared to the conventional SMC (within 3.0% and 2.2%), respectively. Consequently, at transient-state the proposed FASVC reveals a 19 V slighter load voltage-dip and a 0.5 ms faster settling time than the conventional SMC.

TABLE IV

STEADY-STATE AND TRANSIENT-STATE PERFORMANCES OF SIMULATION RESULTS

Case-Studies	**Steady-State Performance**				**Transient-State Performance**			
	THD (%)		**Steady-State Error (%)**		**Load Voltage-Dip (V)**		**Settling Time (ms)**	
	Prop. FASVC	**Conv. SMC**	**Prop. FASVC**	**Conv. SMC**	**Prop. FASVC**	**Conv. SMC**	**Prop. FASVC**	**Conv. SMC**
1	0.30	0.70	0.06	1.09	38	57	0.5	1.0
2	0.35	0.81	0.09	1.27	−	−	−	−
3	1.02	2.80	0.40	2.15	−	−	−	−

4.4 Comparative Experimental Results

In this section, the experimental results of the both proposed FASVC and the conventional SMC are described. Similar to the comparative simulation results, these results are also consider the −30% parameters uncertainties for every case-study, and each figure highlights the waveforms of load voltages (v_{La}, v_{Lb}, v_{Lc}), inverter current (i_{ia}, i_{ib}, i_{ic}), load currents (i_{La}, i_{Lb}, i_{Lc}), estimated load currents (i_{estLa}, i_{estLb}, i_{estLc}), and phase *a* load current error (e_{La}=i_{La}–i_{estLa}).

4.4.1 Case 1: Sudden Load Disturbances

Unlike simulation results, the sudden load disturbances in the experimental results are realized separately due to laboratory test-bed limitations, i.e., full-load to no-load (100%−0%) and no-load to full-load (0%−100%). Fig. 4-8, Fig. 4-9 and Fig. 4-10, Fig. 4-11 respectively describe the performances of the proposed FASVC and conventional SMC under both sudden load disturbances. In depth, Fig. 4-8 shows that the load voltage waveforms are hardly distorted with the zero voltage-dip. Also Figs. 4-9 displays that the load voltages are marginally distorted with a voltage-dip (42 V) and recovered to the steady-state within 0.7 ms. On the other hand, Fig. 4-10 portrays that the load voltages has almost zero voltage-dip. And Fig. 4-11 describes that the load voltage waveforms is distorted with a voltage-dip (66 V) and takes 1.5 ms to be resumed to the steady-state. Thus, it is depicted that the proposed FASVC achieves a smaller voltage-dip and a shorter settling time as compared to the conventional SMC, i.e., (42 V / 66 V and 0.7 ms / 1.5 ms).

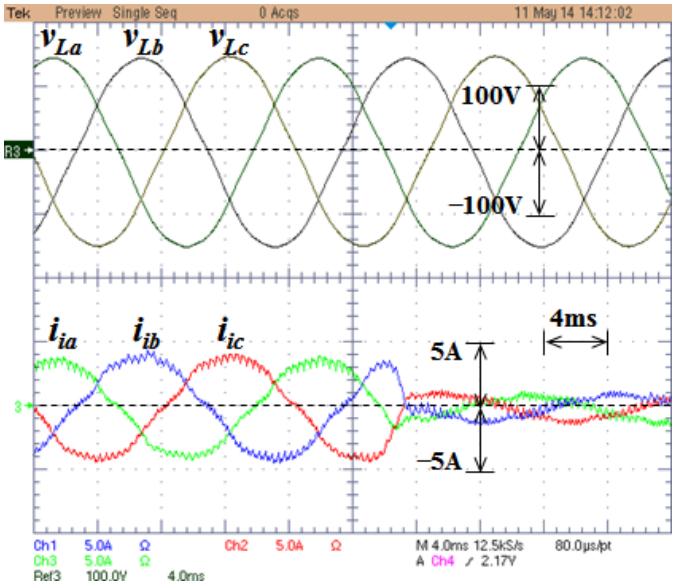

(a)

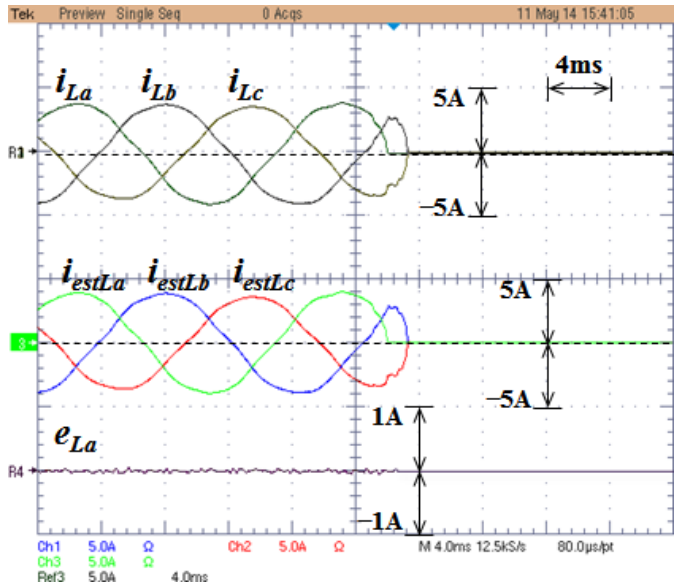

(b)

Fig. 4-8 Experimental results of the proposed FASVC under sudden load disturbance (100%–0%) with –30% parameters uncertainties in L_f and C_f. (a) Load voltages (v_{La}, v_{Lb}, v_{Lc}) and inverter currents (i_{ia}, i_{ib}, i_{ic}). (b) Load currents (i_{La}, i_{Lb}, i_{Lc}), estimated load currents (i_{estLa}, i_{estLb}, i_{estLc}), and phase *a* load current error (e_{La}).

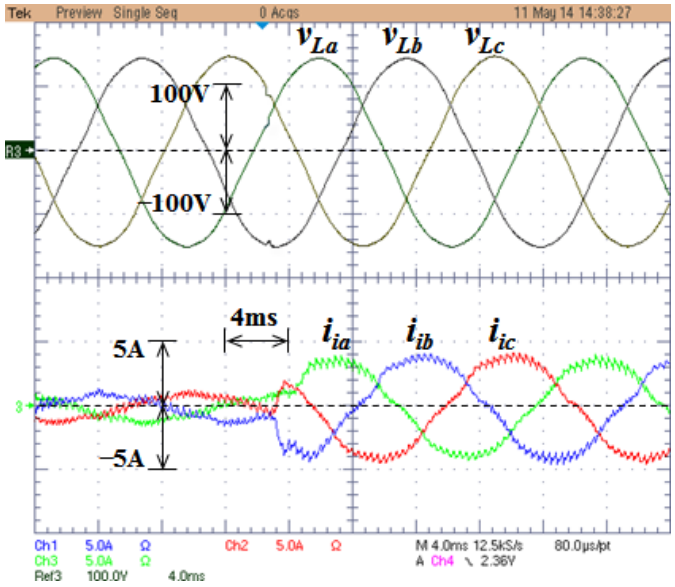

(a)

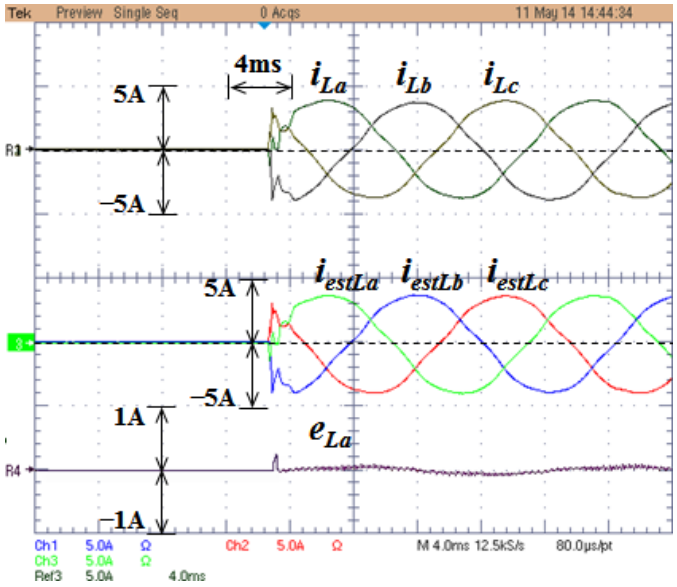

(b)

Fig. 4-9 Experimental results of the proposed FASVC under sudden load disturbance (0%–100%) with –30% parameters uncertainties in L_f and C_f. (a) Load voltages (v_{La}, v_{Lb}, v_{Lc}) and inverter currents (i_{ia}, i_{ib}, i_{ic}). (b) Load currents (i_{La}, i_{Lb}, i_{Lc}), estimated load currents (i_{estLa}, i_{estLb}, i_{estLc}), and phase *a* load current error (e_{La}).

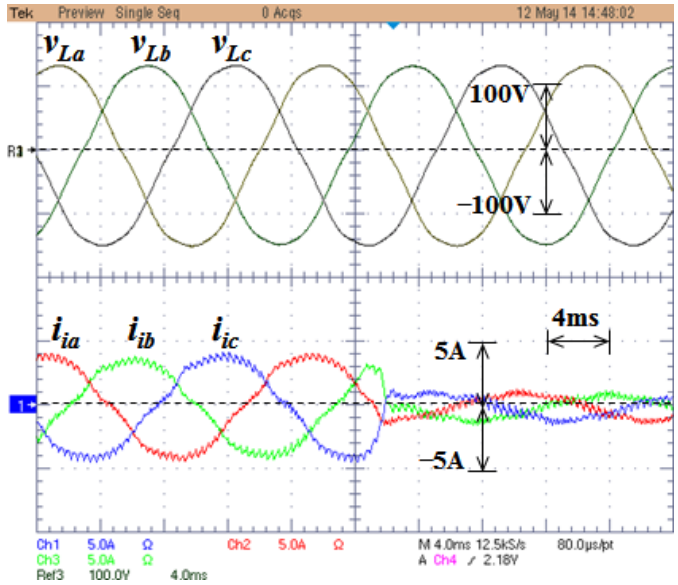

(a)

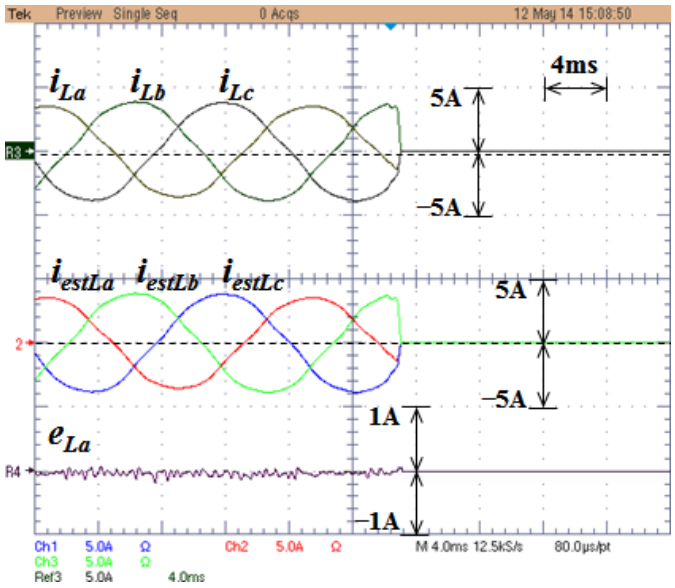

(b)

Fig. 4-10 Experimental results of the conventional SMC under sudden load disturbance (100%–0%) with –30% parameters uncertainties in L_f and C_f. (a) Load voltages (v_{La}, v_{Lb}, v_{Lc}) and inverter currents (i_{ia}, i_{ib}, i_{ic}). (b) Load currents (i_{La}, i_{Lb}, i_{Lc}), estimated load currents (i_{estLa}, i_{estLb}, i_{estLc}), and phase *a* load current error (e_{La}).

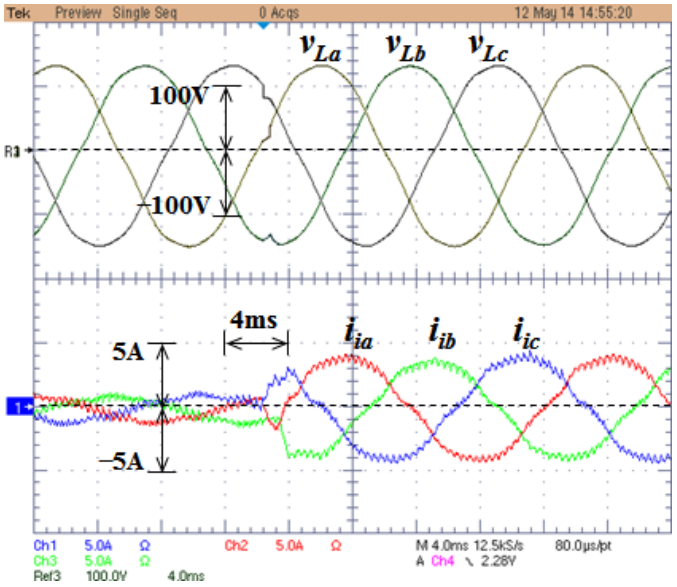

(a)

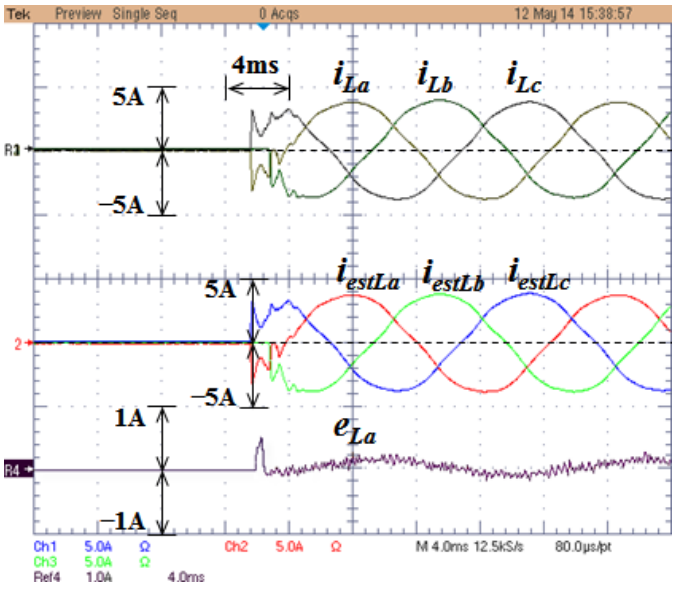

(b)

Fig. 4-11 Experimental results of the conventional SMC under sudden load disturbance (0%–100%) with –30% parameters uncertainties in L_f and C_f. (a) Load voltages (v_{La}, v_{Lb}, v_{Lc}) and inverter currents (i_{ia}, i_{ib}, i_{ic}). (b) Load currents (i_{La}, i_{Lb}, i_{Lc}), estimated load currents (i_{estLa}, i_{estLb}, i_{estLc}), and phase *a* load current error (e_{La}).

4.4.2 Case 2: Sudden Unbalanced Load

Fig. 4-12 and Fig. 4-13 illustrate the experimental results of the proposed FASC and conventional SMC scheme, when an unbalanced resistive load is suddenly applied to the inverter output terminals, i.e., only phase *c* is opened. In detail, the load voltage waveforms of the proposed FASVC presented in Fig. 4-12 look quite sinusoidal compare with the conventional SMC shown in Fig. 4-13. Furthermore, the proposed FASVC exhibits a lesser THD value and the slighter steady-state error than the conventional SMC, i.e., (0.40% / 0.87% and 0.13% / 1.45%).

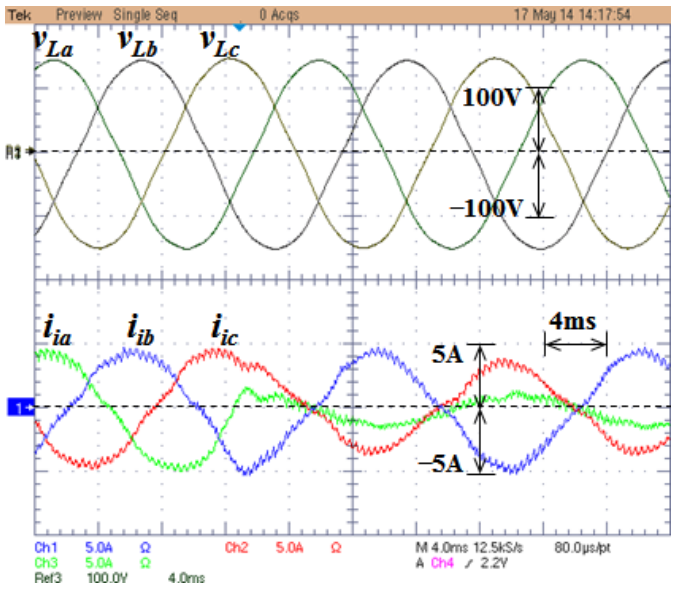

(a)

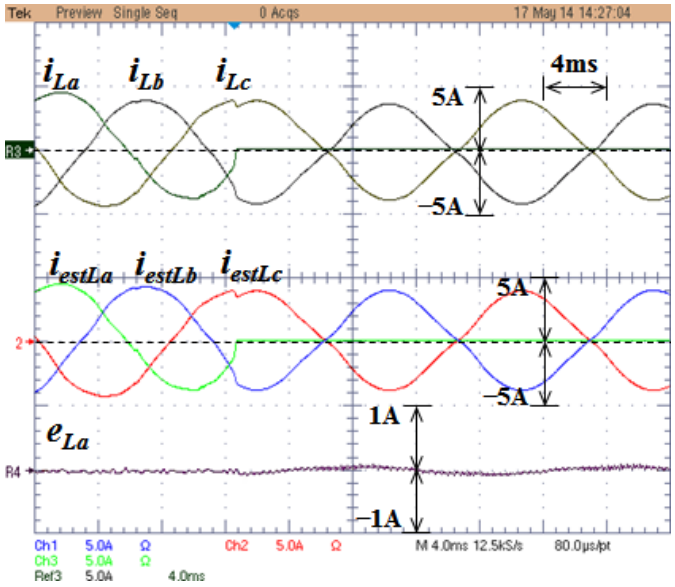

(b)

Fig. 4-12 Experimental results of the proposed FASVC under sudden unbalanced load with –30% parameters uncertainties in L_f and C_f. (a) Load voltages (v_{La}, v_{Lb}, v_{Lc}) and inverter currents (i_{ia}, i_{ib}, i_{ic}). (b) Load currents (i_{La}, i_{Lb}, i_{Lc}), estimated load currents (i_{estLa}, i_{estLb}, i_{estLc}), and phase *a* load current error (e_{La}).

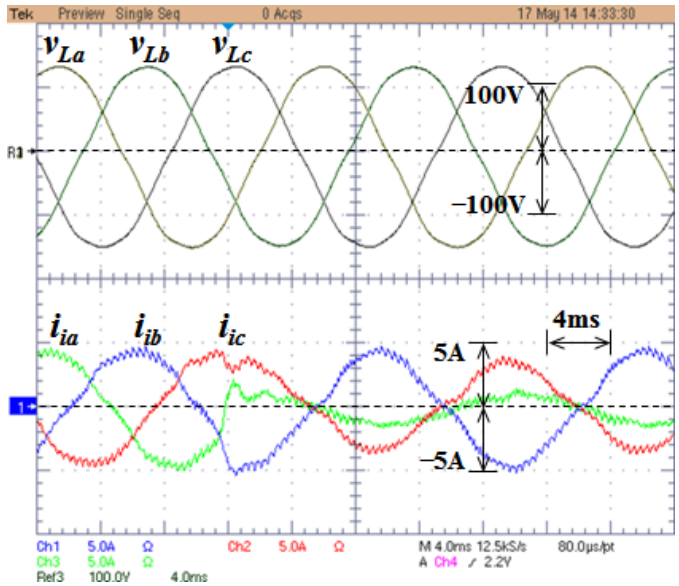

(a)

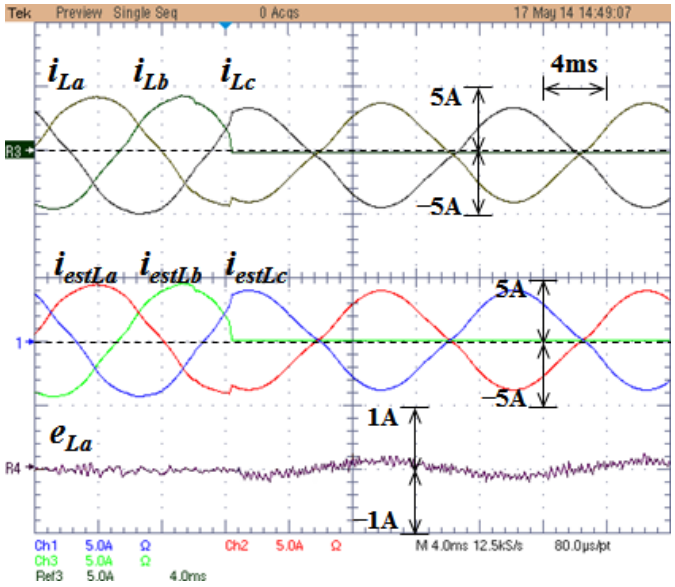

(b)

Fig. 4-13 Experimental results of the conventional SMC under sudden unbalanced load with –30% parameters uncertainties in L_f and C_f. (a) Load voltages (v_{La}, v_{Lb}, v_{Lc}) and inverter currents (i_{ia}, i_{ib}, i_{ic}). (b) Load currents (i_{La}, i_{Lb}, i_{Lc}), estimated load currents (i_{estLa}, i_{estLb}, i_{estLc}), and phase *a* load current error (e_{La}).

4.4.3 Case 3: Nonlinear Load

Fig. 4-14 and Fig. 4-15 present the comparative experimental results, when a nonlinear load of a three-phase full-bridge diode rectifier with parallel *RLC* elements is connected to the inverter output terminals. More precisely, the load voltage waveforms of the proposed FASVC given in Fig. 4-14 reveal a pure sinusoidal behavior than the conventional SMC displayed in Fig. 4-15. Besides the proposed FASVC achieves a THD of 1.08% and a steady-state error of 0.51%, which are respectively smaller as compared to the conventional SMC, i.e., (2.94% and 2.27%).

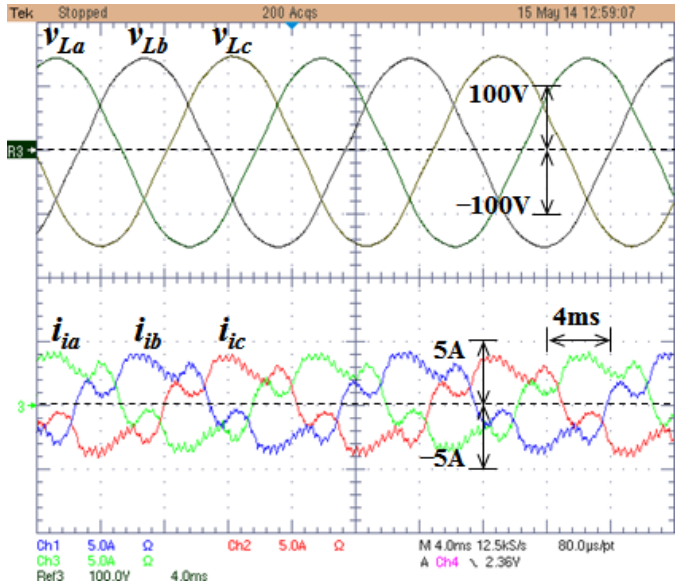

(a)

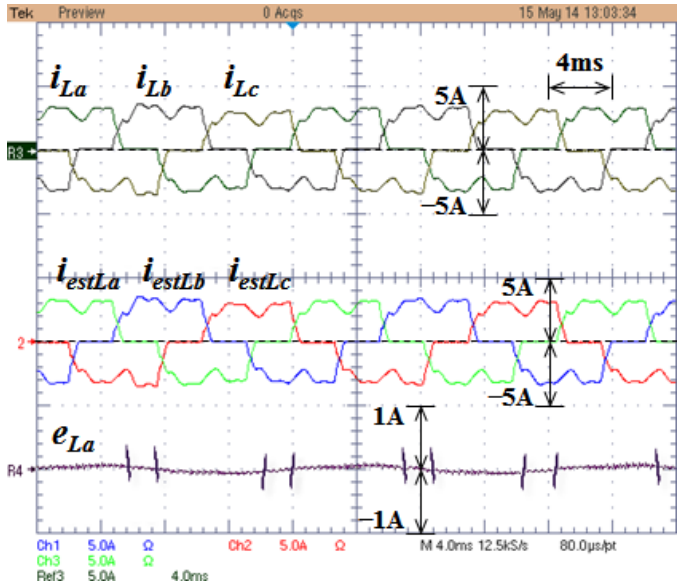

(b)

Fig. 4-14 Experimental results of the proposed FASVC under nonlinear load with –30% parameters uncertainties in L_f and C_f. (a) Load voltages (v_{La}, v_{Lb}, v_{Lc}) and inverter currents (i_{ia}, i_{ib}, i_{ic}). (b) Load currents (i_{La}, i_{Lb}, i_{Lc}), estimated load currents (i_{estLa}, i_{estLb}, i_{estLc}), and phase *a* load current error (e_{La}).

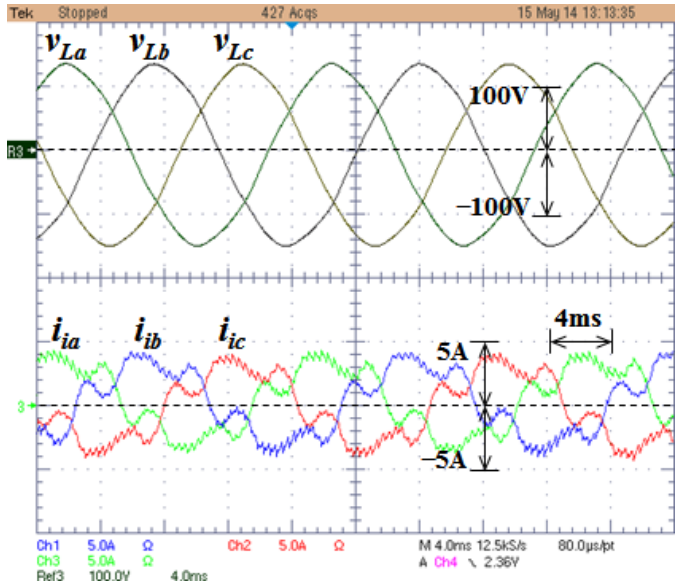

(a)

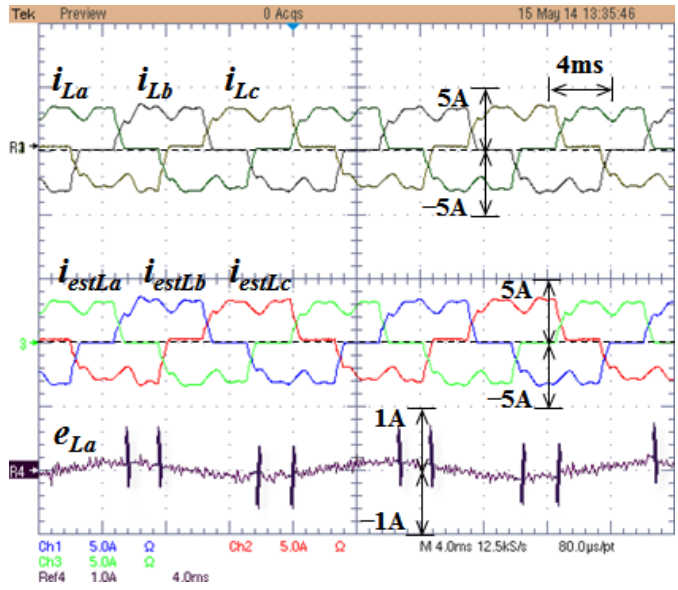

(b)

Fig. 4-15 Experimental results of the conventional SMC under nonlinear load with –30% parameters uncertainties in L_f and C_f. (a) Load voltages (v_{La}, v_{Lb}, v_{Lc}) and inverter currents (i_{ia}, i_{ib}, i_{ic}). (b) Load currents (i_{La}, i_{Lb}, i_{Lc}), estimated load currents (i_{estLa}, i_{estLb}, i_{estLc}), and phase *a* load current error (e_{La}).

.

Table V concludes the superior voltage regulation performance of the proposed FASVC by stating the steady-state and transient-state performances of the comparative experimental results. According to Table V, at steady-state both the THDs and the steady-state errors of the proposed FASVC results a reasonable improvement (within 1.1% and 0.6%) than the conventional SMC (within 3.0% and 2.3%), respectively. Consequently, at transient-state the proposed FASVC exhibits a 24 V slighter load voltage-dip and a 0.8 ms faster settling time as compared to the conventional SMC.

TABLE V

STEADY-STATE AND TRANSIENT-STATE PERFORMANCES OF EXPERIMENTAL RESULTS

Case-Studies	**Steady-State Performance**				**Transient-State Performance**			
	THD (%)		**Steady-State Error (%)**		**Load Voltage-Dip (V)**		**Settling Time (ms)**	
	Prop. FASVC	**Conv. SMC**	**Prop. FASVC**	**Conv. SMC**	**Prop. FASVC**	**Conv. SMC**	**Prop. FASVC**	**Conv. SMC**
1	0.35	0.75	0.09	1.30	42	66	0.7	1.5
2	0.40	0.87	0.13	1.45	–	–	–	–
3	1.08	2.94	0.51	2.27	–	–	–	–

4.5 Summary

In this chapter, the comparative simulation and experimental results were completely presented to verify the excellent steady-state and transient-state performances of the proposed FASVC. Also, a brief description for the prototype setup of a 1 kVA three-phase UPS inverter system and the performance indices was illustrated.

Chapter 5: Conclusions and Future Work

This chapter concludes the whole research work. Also, it presents some suggestions/proposals for the future research work.

5.1 Conclusions

In this thesis, an advanced control approach named as fuzzy adaptive sliding-mode voltage controller (FASVC) for a three-phase UPS inverter was proposed.

First, the power quality issues, main types and performance evaluation criteria of the UPS, and the existing advanced control techniques for the UPS inverter systems were reviewed in the chapter 1.

Second, the chapter 2 derived the mathematical model of the three-phase UPS inverter system including the modeling of three-phase UPS inverter and space vector pulse width modulation (SVPWM).

Next, the design and stability analysis of the proposed fuzzy adaptive sliding-mode voltage controller (FASVC) for the three-phase UPS inverter system were illustrated in the chapter 3.

Finally, the chapter 4 provided the specifications of the developed prototype setup of 1 kVA three-phase UPS inverter system which was simulated by using MATLAB/Simulink software and tested via TMS320F28335 DSP. Furthermore, in this chapter the outstanding performance (i.e., less voltage-dip, quick voltage recovery time, small steady-state error, and low THD) of the proposed FASVC was achieved through the simulation and experimental results in comparison with the

conventional SMC under three case-studies even if there exist the parameter uncertainties.

5.2 Future Work

This thesis proposed an intelligent voltage control strategy of a three-phase inverter for UPS application. However, there are still several proposals for the future research work in terms of the control system design and the focused area/application:

First proposal will be related to the design of a new current observer. As in this research, a conventional current observer is utilized for the load current information. Thus, the addition of a new current observer in the proposed voltage control scheme can improve the performance of three-phase UPS inverter system.

Next proposal will be associated with the extension of the modes of operation within the same application such as parallel operation of the multiple UPS units. In this way, not only the load sharing capacity of the system can be increased but also the reliability of the power delivered to the critical loads can be improved.

Final proposal will be linked to the switching of the focused application such as distributed generation system (DGS). Recently, the DGS research area has become of high interest due to the tendency of smaller and more distributed generation systems using renewable energy sources like wind, electrolysis hydrogen fuel cell, solar, hydro etc. The requirements of the voltage control approach for a three-phase inverter developed in this thesis are the same as those used in a DGS under a stand-alone mode for AC supply. Therefore, the proposed control system can be easily applied to a three-phase stand-alone DGS inverter. In addition, the proposed control system can be extended for other modes of operation in a DGS such as grid-

connected and transitional modes of operation with utility commonly known as parallel operation.

References

[1] R. K. Rojin, "A review of power quality problems and solutions in electrical power system," *IJAREEIE*, vol. 2, no. 11, pp. 5605–5614, Nov. 2013.

[2] B. J. Rahi, V. Vivek, and R. Arumugam, "Harmonics a recent entrant to power quality problem in uninterruptible power supply," *IEEE ICIT, Bangkok, Thailand*, vol. 1, pp. 624–626, Dec. 2002.

[3] J. Lundquist, *On Harmonic Distortion in Power Systems*, Chalmers University of Technology: Department of Electrical Power Engineering, Tech. Report No: 371L, 2001.

[4] S. Roy and L. Umanand, "Integrated magnetics-based multisource quality ac power supply," *IEEE Trans. Ind. Electron.*, vol. 58, no. 4, pp. 1350–1358, Apr. 2011.

[5] J. H. Han, K. Lee, C. S. Song, G. Jang, G. Byeon, and C. H. Park, "A new assessment for the total harmonic contributions at the point of common coupling," *J. Electr. Eng. Technol.*, vol. 9, no. 1, pp. 6–14, Jan. 2014.

[6] H. K. Kang, C. H. Yoo, I. Y. Chung, D. J. Won, and S. I. Moon, "Intelligent coordination method of multiple distributed resources for harmonic current compensation in a microgrid," *J. Electr. Eng. Technol.*, vol. 7, no. 6, pp. 834–844, Nov. 2012.

[7] J. H. Lee, H. G. Jeong, and K. B. Lee, "Performance improvement of grid-connected inverter systems under unbalanced and distorted grid

voltage by using a PR controller," *J. Electr. Eng. Technol.*, vol. 7, no. 6, pp. 918–925, Nov. 2012.

[8] C. Salim, B. M. Toufik, and G. Amar, "Harmonic current compensation based on three-phase three-level shunt active filter using fuzzy logic current controller," *J. Electr. Eng. Technol*., vol. 6, no. 5, pp. 95–604, Sep. 2011.

[9] B. Zhao, Q. Song, W. Liu, and Y. Xiao, "Next-generation multi-functional modular intelligent UPS system for smart grid," *IEEE Trans. Ind. Electron*., vol. 60, no. 9, pp. 3602–3618, Sep. 2013.

[10] A. King and W. Knight, "*Uninterruptible Power Supplies and Standby Power Systems*," USA: McGraw-Hill, 2002.

[11] S. Karve, "Three of a kind," *IEE Review*, vol. 46, no. 2, pp. 27–31, Mar. 2000.

[12] R. Villafafila, "Selection criteria of high-power static uninterruptible power supplies," *IEEE EPQU, Barcelona, Spain*, pp. 1–5, Oct. 2007.

[13] *Uninterruptible power systems (UPS)–Part 3: Method of specifying the performance and test requirements*, IEC Std 62040–3, 2001.

[14] D. Shmilovitz, "On the definition of total harmonic distortion and its effect on measurement interpretation," *IEEE Trans. Power Delivery*, vol. 20, no. 1, pp. 526–528, Jan. 2005.

[15] *IEEE Recommended Practices and Requirements for Harmonic Control in Electrical Power Systems*, IEEE Std 519, 1992.

[16] A. A. McLennan, "High crest factor loads on UPS systems," *IEEE INTELEC, Florence, Italy*, vol. 2, pp. 1–4, Oct. 1989.

[17] A. M. Hava and E. Demirkutlu, "Output voltage control of a four-leg inverter based three-phase UPS," *12th EPE, Aalborg, Denmark*, pp. 1–10, Sep. 2007.

[18] D. E. Kim and D. C. Lee, “Feedback linearization control of three-phase UPS inverter systems,” *IEEE Trans. Ind. Electron.*, vol. 57, no. 3, pp. 963–968, Mar. 2010.

[19] G. Escobar, A. M. Stankovic, and P. Mattavelli, “An adaptive controller in stationary reference frame for D-statcom in unbalanced operation,” *IEEE Trans. Ind. Electron.*, vol. 51, no. 2, pp. 401–409, Apr. 2004.

[20] R. Escobar, A. A. Valdez, J. Leyva-Ramos, and P. Mattavelli, “Repetitive-based controller for a UPS inverter to compensate unbalance and harmonic distortion,” *IEEE Trans. Ind. Electron.*, vol. 54, no. 1, pp. 504–510, Feb. 2007.

[21] P. Cortés, G. Ortiz, J. I. Yuz, J. Rodrisguez, S. Vazquez, and L. G. Franquelo, “Model predictive control of an inverter with output *LC* filter for UPS applications,” *IEEE Trans. Ind. Electron.*, vol. 56, no. 6, pp. 1875–1883, Jun. 2009.

[22] P. C. Loh, M. J. Newman, D. N. Zmood, and D. G. Holmes, “A comparative analysis of multiloop voltage regulation strategies for single and three-phase UPS systems,” *IEEE Trans. Power Electron.*, vol. 18, no. 5, pp. 1176–1185, Sep. 2003.

[23] C. Li, S. M. Ji, and D. P. Tan, “Multiple-loop digital control method for a 400-Hz inverter system based on phase feedback,” *IEEE Trans. Power Electron.*, vol. 28, no. 1, pp. 408–417, Jan. 2013.

[24] M. Kojima, K. Hirabayashi, and Y. Kawabata, “Novel vector control system using deadbeat-controlled PWM inverter with output *LC* filter,” *IEEE Trans. Ind. Appl.*, vol. 40, no. 1, pp. 162–169, Jan/Feb. 2004.

[25] P. Mattaveli, “An improved deadbeat control for UPS using disturbance observers,” *IEEE Trans. Ind. Electron.*, vol. 52, no. 1, pp. 206–212, Feb. 2005.

[26] T. S. Lee, S. J. Chiang, and J. M. Chang, "H_∞ loop-shaping controller designs for the single-phase UPS inverters," *IEEE Trans. Power Electron.*, vol. 16, no. 4, pp. 473–481, Jul. 2001.

[27] F. Y. Hsu and L. C. Fu, "Adaptive fuzzy control for uninterruptible power supply with three-phase PWM inverter," *IEEE Proc. AFSS, Kenting, Taiwan*, pp. 188–193, Dec. 1996.

[28] D. S. Xu, K. Yong, and C. Jian, "An algorithm for the output waveform compensation of SPWM inverters based on fuzzy-repetitive control," *J. Electr. Eng.*, vol. 55, no. 3/4, pp. 64–70, 2004.

[29] O. Kukrer, H. Komurcugil, and A. Doganalp, "A three-level hysteresis function approach to the sliding-mode control of single-phase UPS inverters," *IEEE Trans. Ind. Electron.*, vol. 56, no. 9, pp. 3477–3486, Sep. 2009.

[30] H. Komurcugil, "Rotating sliding line based sliding-mode control for single-phase UPS inverters," *IEEE Trans. Ind. Electron.*, vol. 59, no. 10, pp. 3719–3726, Oct. 2012.

[31] R. J. Wai and C. Y. Lin, " Dual active low-frequency ripple control for clean-energy power-conditioning mechanism," *IEEE Trans. Ind. Electron.*, vol. 58, no. 11, pp. 5172–5185, Nov. 2011.

[32] M. Dai, M. N. Marwali, J. W. Jung, and A. Keyhani, "A three-phase four-wire inverter control technique for a single distributed generation unit in island mode," *IEEE Trans. Power Electron*., vol. 23, no. 1, pp. 322–331, Jan. 2008.

[33] M. N. Marwali and A. Keyhani, "Control of distributed generation systems–part I: voltages and currents control," *IEEE Trans. Power Electron.*, vol. 19, no. 6, pp. 1541–1550, Nov. 2004.

[34] *Clarke & Park Transform on the TMS320C2xx*, TEXAS INSTRUMENTS, LN: BPRA048, 1997.

[35] S. Chattopadhyay, S. Sengupta, and M. Mitra, *Electric Power Quality*, Springer. 2011.

[36] H.W. Van Der Broeck, H. C. Skudelny, and G.V. Stanke, "Analysis and realization of a pulsewidth modulator based on voltage space vectors," *IEEE Trans. Ind. App.*, vol. 24, pp. 142–150, Jan/Feb. 1988.

[37] B. P. McGrath, D. G. Holmes, and T. Lipo, "Optimized space vector switching sequences for multilevel inverters," *IEEE Trans. Power Electron.*, vol. 18, no. 6, pp. 1293–1301, Nov. 2003.

[38] S. Singh and K. S. Rattan, "Implementation of a fuzzy logic controller on an FPGA for a DC motor," *IEEE Proc. EICEME*, pp. 387–394, Sep. 2003.

[39] C. C. Lee, "Fuzzy logic in control system: Fuzzy logic controller–Part I," *IEEE Trans. Syst., Man, Cybern.*, vol. 20, no. 2, pp. 404–418, Mar./Apr. 1990.

[40] B. Yoo and W. Ham, "Adaptive fuzzy sliding mode control of nonlinear system," *IEEE Trans. Fuzzy Syst.*, vol. 18, no. 6, pp. 1293–1301, Nov. 2003.

[41] J. L. Castro, "Fuzzy logic controllers are universal approximators," *IEEE Trans. Syst. Man. Cybern.*, vol. 25, no. 4, pp. 629–635, 1995.

[42] L. X. Wang, "Stable adaptive fuzzy control of nonlinear systems," *IEEE Trans. Fuzzy Syst.*, vol.1, no.2, pp. 146–155, 1993.

[43] R. A. DeCarlo, S. H. Zak, and G. P. Mathews, "Variable structure control of nonlinear multivariable systems: a tutorial," *IEEE Proc.*, vol. 76, no.3, pp. 212–232, Mar. 1988.

[44] H. Khalil, *Nonlinear Systems*, New Jersey: Prentice-Hall Inc., 2003.

[45] F. L. Lewis, C. T. Abdallah, and D. M. Dawson, *Control of Robot Manipulators*, New York: MacMillan, 1993.

[46] H. H. Choi, "Adaptive controller design for uncertain fuzzy systems

using variable structure control approach," *Automatica,* vol. 45, no. 11, pp. 2646–2650, Jul. 2009.

[47] W. S. Lin and C. S. Chen, "Robust adaptive sliding-mode control using fuzzy modelling for a class of uncertain MIMO nonlinear systems," *IEE Proc-Control Theory and Appl*., no. 149, pp. 193–201, Aug. 2002.

[48] K. J. Astrom and B. Witternmark, *Computer-Controlled Systems–Theory and Design*, Englewood Cliffs, New Jersey: Prentice-Hall Inc, 1990.

[49] F. Lin, *Robust Control Design: An Optimal Control Approach*, England: John Wiley and Sons Ltd., 2007.

[50] H. Kim and S. K. Sul, "A novel filter design for output *LC* filters of PWM inverters," *Journal of Power Electron.,* vol. 11, no. 1, pp. 74–81, Jan. 2011.

[51] I. A. Hameed, "Using Gaussian membership functions for improving the reliability and robustness of students' evaluation systems," *ELSEVIER Expert Systems with Appl.*, vol. 38, no. 6, pp. 7135–7142, Jun. 2011.

[52] H. Zumbahlen, *Linear Circuit Design Handbook*, Analog Devices Inc. Engineering, Newnes, Ch. 10, 2008.

Publication

---

[1] **Khawar Naheem**, Young-Sik Choi, Francis Mwasilu, Han Ho Choi, and Jin-Woo Jung, "Design and stability analysis of fuzzy adaptive SMC system for three-phase UPS inverter," *Journal of Power Electron.*, vol. 14, no. 4, pp. 704–711, Jul. 2014.